HAL
open science

THz spectroscopy and first ISM detection of excited torsional states of 13C-methyl formate

I., Haykal, M., Carvajal, B., Tercero, I., Kleiner, A., López, J., Cernicharo, R. A., Motiyenko, T. R., Huet, J. C., Guillemin, L., Margulès

To cite this version:

I., Haykal, M., Carvajal, B., Tercero, I., Kleiner, A., López, et al.. THz spectroscopy and first ISM detection of excited torsional states of 13C-methyl formate. Astronomy and Astrophysics - A&A, 2014, 568, pp.A58. 10.1051/0004-6361/201322937 . hal-01133043

HAL Id: hal-01133043

https://univ-rennes.hal.science/hal-01133043v1

Submitted on 5 Nov 2022

HAL is a multi-disciplinary open access archive for the deposit and dissemination of scientific research documents, whether they are published or not. The documents may come from teaching and research institutions in France or abroad, or from public or private research centers.

L'archive ouverte pluridisciplinaire **HAL**, est destinée au dépôt et à la diffusion de documents scientifiques de niveau recherche, publiés ou non, émanant des établissements d'enseignement et de recherche français ou étrangers, des laboratoires publics ou privés.

A&A 568, A58 (2014)
DOI: 10.1051/0004-6361/201322937
© ESO 2014

Astronomy & Astrophysics

THz spectroscopy and first ISM detection of excited torsional states of ^{13}C-methyl formate*

I. Haykal[1], M. Carvajal[2], B. Tercero[3], I. Kleiner[4], A. López[3], J. Cernicharo[3], R. A. Motiyenko[1], T. R. Huet[1], J. C. Guillemin[5], and L. Margulès[1]

[1] Laboratoire de Physique des Lasers, Atomes, et Molécules, UMR CNRS 8523, Université Lille I, 59655 Villeneuve d'Ascq Cedex, France
e-mail: laurent.margules@univ-lille1.fr
[2] Departamento de Física Aplicada Unidad Asociada CSIC, Facultad de Ciencias Experimentales, Universidad de Huelva, 21071 Huelva, Spain
[3] Centro de Astrobiología (CSIC-INTA), Department of Astrophysics. Ctra de Ajalvir, 28850 Torrejón de Ardoz, Madrid, Spain
[4] Laboratoire Interuniversitaire des Systèmes Atmosphériques, UMR CNRS/IPSL 7583, Université Paris 7 et Université Paris Est, 61 Av. Charles de Gaulle, 94010 Créteil Cedex, France
[5] Institut des Sciences Chimique de Rennes, École Nationale Supérieure de Chimie de Rennes, CNRS, UMR 6226, Allée de Beaulieu, CS 50837, 35708 Rennes Cedex 7, France

Received 29 October 2013 / Accepted 24 April 2014

ABSTRACT

Context. An astronomical survey of interstellar molecular clouds needs a previous analysis of the spectra in the microwave and sub-mm energy range of organic molecules to be able to identify them. We obtained very accurate spectroscopic constants in a comprehensive laboratory analysis of rotational spectra. These constants can be used to predict the transitions frequencies very precisely that were not measured in the laboratory.

Aims. We present the experimental study and its theoretical analysis for two ^{13}C-methyl formate isotopologues to detect these two isotopologues for the first time in their excited torsional states, which lie at 130 cm^{-1} (200 K) in Orion-KL.

Methods. New spectra of HCOO^{13}CH$_3$ (^{13}C$_2$) methyl formate were recorded with the mm- and submm-wave spectrometer in Lille from 50 to 940 GHz. A global fit for $v_t = 0$ and 1 was accomplished with the BELGI program to reproduce the experimental spectra with greater accuracy.

Results. We analysed 5728 and 2881 new lines for $v_t = 0$ and 1 for HCOO^{13}CH$_3$. These new lines were globally fitted with 846 previously published lines for $v_t = 0$. In consequence, 52 parameters of the RAM Hamiltonian were accurately determined and the value of the barrier height (V_3 = 369.93168(395) cm^{-1}) was improved. We report the detection of the first excited torsional states ($v_t = 1$) in Orion-KL for the ^{13}C$_2$ and ^{13}C$_1$ methyl formate based on the present analysis and previously published data. We provide column densities, isotopic abundances, and vibrational temperatures for these species.

Conclusions. Following this work, accurate prediction can be provided. This permits detecting 135 features of the first excited torsional states of ^{13}C-methyl formate isotopologues in Orion-KL in the 80−280 GHz frequency range, without missing lines.

Key words. line: identification – astronomical databases: miscellaneous – ISM: molecules – submillimeter: ISM – astrochemistry – ISM: individual objects: Orion KL

1. Introduction

Methyl formate is one of the most abundant complex organic molecules in the interstellar medium (ISM). It was identified in different sources since 1975 (Brown et al. 1975; Churchwell et al. 1975); nearly one thousand lines were detected in the ground-torsional state $v_t = 0$. Its abundance is particularly high in Orion-KL: it was detected up to 900 GHz (Comito et al. 2005) far from the maximum of absorption situated around 300 GHz; some lines from the first (Kobayashi et al. 2007), and more recently, lines from the second torsional state were detected (Takano et al. 2012). The abundance is also fairly high in W51e2, where lines from methyl formate in its first torsional states were found (Demyk et al. 2008). Molecules in the ISM can be used to probe the physical conditions of sources, as illustrated recently by Favre et al. (2011, 2014) using methyl formate to probe the temperature structure and spatial distribution of this species in Orion-KL; depending on the molecular species, the distribution of the molecular gas can be different in this source because of its complexity (which is a result of massive star formation processes) different cloud components coexist there. Organic saturated O-rich molecules such as methyl formate generally trace the compact ridge component (for a description of the different cloud components of Orion-KL see e.g. Blake et al. 1987; Schilke et al. 2001; Persson et al. 2007; Tercero et al. 2010, 2011; Neill et al. 2013).

Around 180 molecules have been detected in the ISM or circumstellar shells, but in high mass-forming regions such as Orion-KL, 30% of the lines remain unidentified (Esplugues et al. 2013a; Tercero et al. 2010). Its important to identify all the lines from the most abundant species. These molecules are often called "weeds", and methyl formate is one of them.

* Full Table A.1 and the IRAM spectra as FITS files are only available at the CDS via anonymous ftp to cdsarc.u-strasbg.fr (130.79.128.5) or via http://cdsarc.u-strasbg.fr/viz-bin/qcat?J/A+A/568/A58

Identifying them is necessary in order to discover new species in the ISM without ambiguity. As shown recently by Tercero et al. (2013), the detection of methyl acetate (CH_3COOCH_3) and the gauche conformer of ethyl formate (g-CH_3CH_2OCOH) was only possible with the assignment of 4400 lines coming from several isotopologues and vibrational levels of different weeds: CH_3CH_2CN, CH_2CHCN, $HCOOCH_3$, and NH_2CHO.

Most of the times, accurate spectroscopic data in the millimeter and submillimeter-wave domain are not available for the isotopologues and vibrational levels. While the normal species of methyl formate were extensively studied (Ilyushin et al. 2009, and references therein) of only the two commercially available isotopologues $H^{13}COOCH_3$ (Maeda et al. 2008a,b) and $DCOOCH_3$ (Oesterling et al. 1995) were studied in the millimeter-wave region. Therefore we decided to investigate all the mono-isotopic species of methyl formate in the submillimeter-wave domain a few years ago. For each of them, this permits generating a new accurate prediction and allows detecting the ^{13}C species (Willaert et al. 2006; Carvajal et al. 2007, 2009, 2010), $DCOOCH_3$ (Margulès et al. 2010), ^{18}O species (Tercero et al. 2012) in Orion-KL and recently $HCOOCH_2D$ (Coudert et al. 2013). This confirms the assumption that most of the U-lines come from known molecules. The lines detected for the ^{18}O species gave us the idea that it might also be possible to find lines related to the first excited torsional states that lie at 130 cm^{-1} (200 K) of the most abundant isotopologues ^{13}C.

Our motivations for studying of the first excited torsional state of $HCOO^{13}CH_3$ is also linked to a spectroscopic interest. Methyl formate, like other complex molecules, exhibits large-amplitude motion: torsion of the methyl group related to the rest of the molecules. A specific code that takes into account the interaction of the torsion and the overall rotation of the molecule is needed. Most of the codes were developed to treat data in the centimeter not in millimeter-wave domain. Recent efforts from different theoretical groups were recently make to improve the codes to reproduce the experimental accuracies with high quantum numbers that are reached at submillimeter frequencies. As shown for the normal species (Ilyushin et al. 2009) and the $^{13}C_1$ species (Carvajal et al. 2010), the global treatment of the ground- and first torsional states permits removing the high correlation between torsional parameters. This improves the quality of the fit and finally the accuracy of the predictions for the two states.

These works permit the first detection of the excited torsional state of the two ^{13}C-methyl formate isotopologues. As in Carvajal et al. (2009), we publish the spectroscopic work about $HCOO^{13}CH_3$ and the detection of the two ^{13}C isotopologues in Orion together. In the previous paper about $^{13}C_2$ (Carvajal et al. 2009), our measurements were limited to 660 GHz for the ground-torsional states. To provide an accurate prediction of this state in the ALMA range, we also reinvestigated this state up to 940 GHz.

2. Experiments

2.1. Synthesis of the methyl formate isotopologue $HCOO^{13}CH_3$

The details about synthesis and identification by NMR spectroscopy were described in Carvajal et al. (2009).

2.2. Lille – submillimeter spectra

The millimeter- and submillimeter-wave spectra were recorded using the Lille spectrometer that is based on solid-state sources (Motiyenko et al. 2010; Haykal et al. 2013a). The sample pressure was in the range $20-30 \times 10^{-6}$ bars. Spectra were recorded at room temperature (T = 294 K) in the 150−210, 225−315, 400−500, 500−630, and 780−940 GHz regions with frequency steps of 30, 36, 48, 54, and 76 kHz and an acquisition time of 35 ms per point. Absorption signals were detected either by a Schottky diodes detector (Virginia Diodes Inc.) below 315 GHz or by an InSb liquid He-cooled bolometer (QMC Instruments Ltd.) above 400 GHz, and were processed on a computer. The absolute accuracy of the line-centre frequency is estimated to be better than 30 kHz (50 kHz above 700 GHz) for isolated lines and can be as low as 100 kHz (150 kHz above 700 GHz) for blended or very weak lines.

3. Assignments and fit of the $HCOO^{13}CH_3$ spectrum

The theoretical model and the so-called RAM method (rho-axis method) used for the present spectral analyses and fits of the ground- and first torsional-excited states of $HCOO^{13}CH_3$ species have also been used previously for a number of molecules that contain an internal methyl rotor (see for example Ilyushin et al. 2003, 2008) and in particular for the normal species of the cis-methyl formate (Carvajal et al. 2007; Ilyushin et al. 2009), the two ^{13}C species (Carvajal et al. 2009, 2010), for $DCOOCH_3$ (Margulès et al. 2010), and for ^{18}O species (Tercero et al. 2012). The RAM Hamiltonian we used is based on previous works (Kirtman 1962; Lees & Baker 1968; Herbst et al. 1984). Because this method has been presented in great detail in the literature (Lin & Swalen 1959; Hougen et al. 1994; Kleiner 2010), we do not describe it here. The principal advantage of the RAM general approach used in our code BELGI, which is publicly available[1], is its general approach that simultaneously takes into account the A- and E-symmetry states in our fit. All the torsional levels up to a truncation limit of v_t = 8 are carefully tested and the interactions within the rotation-torsion energy levels are also included in the rotation-torsion Hamiltonian matrix elements (Kleiner et al. 1996). The various rotational, torsional, and coupling terms between rotation and torsion that we used for the fit of the $HCOO^{13}CH_3$ species were defined previously for the normal methyl formate species (Carvajal et al. 2007). The labelling scheme of the energy levels and transitions used for methyl formate was also described in the same reference, as was the connection with the more traditional J_{K_a,K_c} labelling.

We started with the assignment of the ground state. Predictions were provided by the BELGI program based on the set of 27 parameters previously determined in Carvajal et al. (2009). In this reference, only 658 lines were assigned from 150 to 700 GHz. Our new spectrometer has a wider coverage range than that used in 2009. Based on the previous work, we easily assigned the spectra up to J = 63 and K_a = 34 in the range 75−630 GHz. In the highest frequency range of the mm- and submm- wave spectrometer (700−940 GHz), the assignment was tentative because of the shift of the predicted lines from the experimental lines. The upper limit in frequency of the 936 previously fitted lines was 700 GHz. As a result, we assigned for the ground-state 5728 lines up to J = 60 and K_a = 35 from 50 to 940 GHz. Next, we started up again, but simultaneously including data of states v_t = 0 and v_t = 1. The fit was carried out in

[1] The source code for the fit, an example of input data file, and a readme file are available at the web site (http://www.ifpan.edu.pl/~kisiel/introt/introt.htm#belgi) managed by Zbigniew Kisiel. Extended versions of the code made to fit transitions with higher J and K are also available from the authors (I. Kleiner and M.C.).

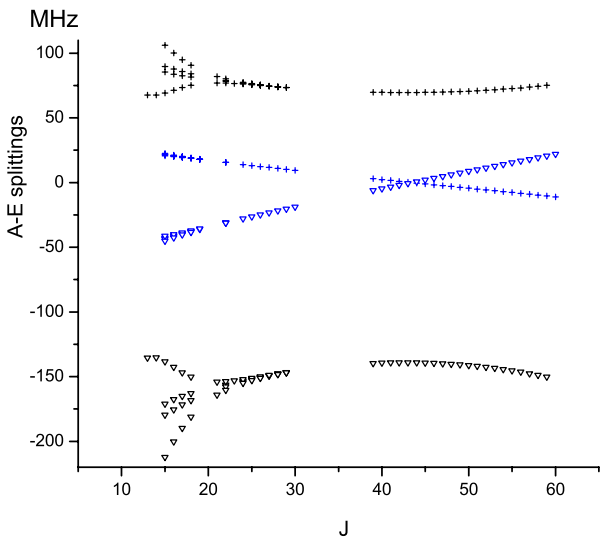

Fig. 1. A-E splitting of selected branches (R branches for $K_a = 0; 1$ in blue and 1;2 in black) for $v_t = 1$. The x-axis represents the situation without perturbation. The A transitions (▽ signs) are twice as far as the E transitions (+ signs). For $K_a = 0; 1$ the A-E splitting changes sign at $J = 44$ (Ilyushin et al. 2009).

these two steps to avoid any possible misassignments. The improvement of the fit is then based on the variety and richness of the data set, and the addition of lines belonging to $v_t = 1$ is crucial. The analysis of the first excited torsional state was challenging because of a larger splitting of the A and E component by the tunnelling effect. In a recent work by Tudorie et al. (2012) the band origins ($E_A = 132.4303$ cm^{-1} and $E_E = 131.8445$ cm^{-1}) for $v_t = 1$ of the parent molecule were precisely determined by a combination of microwave, mm-wave, submm-wave, and far infrared data. The value of height of the barrier was as much improved and V_3 was determined to be equal to 370.7398 (58) cm^{-1}. In this work, for HCOO^{13}CH$_3$, the first torsional excited substates are predicted to be $E_A = 131.0565$ cm^{-1} and $E_E = 130.4856$ cm^{-1}. We estimated the rotational parameters using the same difference of the ground- and the first-torsional excited states rotational parameters of the ^{12}C species. In the assignment procedure, the a-type transitions with A symmetry of R-branches were first analysed, in particular, the most intense lines with $K_a = 0$ and 1.

Methyl formate is a fairly asymmetric near-prolate top for which the dipole moment is non-zero along the a and b principle axis. For the parent specie, μ_a and μ_b were measured by Margulès et al. (2010) and their values are 1.648(8) and 0.706(12) D. We tracked these transitions based on the intensity criterion. Next we assigned the E type of transitions with the same benchmarks as those adopted for the A type of transitions. For K_a the splitting between the A transitions, as well as between the E transitions, decreases with the increase of the J quantum number. Four μ_a and μ_b rotational transitions with the same symmetry (A or E) become blended at $J = 24$. Furthermore, in the mm-wave ranges the splitting between the A and E transitions decreases with the increase of J and at a specific value of J in the submm-wave ranges this splitting changes sign (Fig. 1). Following this behaviour of the A and E type of transition for $K_a = 0$ and 1, we assigned them up to $J = 50$ at ~520 GHz. We fitted these for $v_t = 1$ with the ERHAM (Groner 1997, 2012) program. The predictions based on this first fit were accurate enough to continue and to search for higher quantum number lines. We collected 800 A lines and 596 E lines with $K_{a,\max} = 19$ and 11 up to $J = 50$ for the A and E lines. ERHAM[2] treats each torsional state separately, and to proceed with the global analysis of $v_t = 0$ and 1, we used BELGI. The final data set with the upper limits of the quantum numbers and the experimental uncertainties are summarized in Table 1. The 6574 lines belonging to $v_t = 0$ and 2881 lines belonging to $v_t = 1$ were fitted with root-mean-square deviations of 38.3 and 41.9 kHz. The fit of the total of 9455 lines for $v_t = 0$ and 1 of A and E symmetries resulted in the determination of 52 parameters of the RAM Hamiltonian. Table 3 presents the values of the set of 52 newly determined parameters. In this table we also provide a comparison with the previous work. Principally, we note a striking change in the value of the barrier height. The value of the parameter V_3 changed from 407.1549(147) to 369.93168(395) cm^{-1}.

The reason for this is the fact that this parameter is an effective value. In the previous fit (Carvajal et al. 2009), the data set of lines concerned only the $v_t = 0$ state and, therefore, neither the second-order parameter (V_6) of the torsional potential function nor the kinetic parameter F could be determined. Then, F was fixed to a relatively high value estimated by ab initio methods, and in the fitting procedure, the effective value of V_3 absorbed the error of F and contained the contribution of V_6:

$$V(\gamma) = \frac{V_3}{2} \times (1 - \cos 3\gamma) + \frac{V_6}{2} \times (1 - \cos 6\gamma) + \ldots$$

The new combination of data from $v_t = 0$ and 1 improved the quality of the fit and allowed determining of 25 new parameters, particularly F and V_6.

4. Line strengths

The intensity calculations for the two ^{13}C species of methyl formate were performed using the same method described in Hougen et al. (1994) and Ilyushin et al. (2008), that was applied for the normal species by Carvajal et al. (2007), the ^{13}C species (Carvajal et al. 2009, 2010), DCOOCH$_3$ (Margulès et al. 2010), and ^{18}O species (Tercero et al. 2012). For this reason we do not repeat it here. The line strength calculation for the ^{13}C species was performed using the same value for the dipole moment as for the parent methyl formate (Margulès et al. 2010). This assumption was made because the angle between the internal axis of the methyl top and the principal a-axis does not change much upon substitution (see the $<(i, a)$ angle values in Table 3). All other structural parameters such as the angle between RAM and PAM axes ($\theta_{\rm RAM}$) and the ρ parameter do not change much upon substitution (see Table 3). Because the changes in the structure in the various isotopomers are not important, we assumed that the dipole moment does not change considerably from one species to another. The dipole moment components of H^{13}COOCH$_3$ (Carvajal et al. 2010) and HCOO^{13}CH$_3$ in RAM axis system that we used for the intensity calculations are $\mu_a^{\rm RAM} = 1.792$ D; $\mu_b^{\rm RAM} = -0.044$ D and $\mu_a^{\rm RAM} = 1.793$ D; $\mu_b^{\rm RAM} = -0.022$D, respectively. We provide Table A.1, which is part of the supplementary Table S (available on CDS). It contains all included lines from our fit for the HCOO^{13}CH$_3$ methyl formate species. They show the line assignments, the observed frequencies with measurement uncertainty (in parenthesis), the computed frequencies, observed-calculated values, the line strength, and the lower-state energy relative to the $J = K = 0$ A-species level taken as zero-energy level. The prediction line-list of all transitions in $v_t = 0$ and 1 will be transmitted to the SPLATALOG and CDMS database (available at www.splatalogue.net).

[2] http://www.ifpan.edu.pl/~kisiel/introt/introt.htm#erham

Table 1. Root-mean-square (rms) deviations from the global fit[a] of transitions involving $v_t = 0$ and $v_t = 1$ torsional energy levels of $^{13}C_2$-methyl formate ($HCOO^{13}CH_3$).

Number of parameters				52	
Number of lines				9455	
rms of the 6574 MW $v_t = 0$–0 lines				0.0383 MHz	
rms of the 2881 MW $v_t = 1$–1 lines				0.0419 MHz	
rms of the 5184 A symmetry lines				0.0429 MHz	
rms of the 4271 E symmetry lines				0.0349 MHz	
Source[b]	Range[c] (GHz)	v_t, J_{max}, K_{max}[d]	Number of lines[e]	Uncertainties[f] (MHz)	rms[g] (MHz)
AA09	4–20	0, 7, 3	27	0.005	0.0056
AA09	150–700[j]	0, 63, 35	607	0.030	0.0252
NEW	50–940[k]	0, 60, 35	4864	0.030	
NEW	50–940[k]	1, 60, 26	1731	0.030	
AA09	150–700[j]	0, 52, 27	2	0.050	
NEW	50–940[k]	0, 52, 35	577	0.050	
NEW	50–940[k]	1, 58, 26	814	0.050	
AA09	8–700[j]	0, 58, 29	43	0.100[h]	0.0644
NEW	50–940[k]	0, 55, 33	170	0.100[i]	
NEW	50–940[k]	1, 57, 26	203	0.100[i]	
AA09	8–700[j]	0, 33, 11	122	0.150[h]	0.1345
NEW	50–940[k]	0, 54, 33	49	0.150[i]	
NEW	50–940[k]	1, 55, 24	68	0.150[i]	
AA09	8–700[j]	0, 58, 25	45	0.200[h]	
NEW	50–940[k]	0, 55, 31	68	0.200[i]	
NEW	50–940[k]	1, 55, 20	65	0.200[i]	

Notes. [(a)] Parameter values are given in Table 2. The complete list of observed minus calculated residuals of $v_t = 0$ lines are given in the supplementary Table A.1. [(b)] Sources of data: AA09 stands for Carvajal et al. (2009) and NEW data come from the present work. The spectroscopic instruments are described in Sect. 2.2. [(c)] Spectral range of the measurements. [(d)] Torsional state v_t, maximum J and K_a for each group of measurements. [(e)] Number of MW lines in each uncertainty group. [(f)] Uncertainty in MHz used in the fit. [(g)] Root-mean-square deviation in MHz for each group. [(h)] The details of the accuracy of spectral measurements are given in Carvajal et al. (2009). [(i)] The accuracy of spectral measurements for the Lille spectrometer is about 0.030 MHz for isolated lines but some lines are either blended or present a poor S/N ratio and therefore their measurement accuracy is taken as either 0.100 MHz, 0.150 MHz or 0.200 MHz according to the broadening of the experimental line. [(j)] The spectrometer spectral ranges for these measurements are 8−80 GHz, 150−245 GHz, 320−350 GHz, 510−525 GHz, and 580−661 GHz (for more details, see Carvajal et al. 2009). [(k)] The spectrometer spectral ranges for the measurements of present work are: 50−100 GHz and 150−940 GHz, using a multiplication chain of solid state sources, and 100−150 GHz, using a backward wave oscillator.

5. Detection of ^{13}C-HCOOCH$_3$ $v_t = 1$ in Orion KL

In this section we use the notation ^{13}C-HCOOCH$_3$ when we refer to the two isotopologues. Following the procedure of our previous papers, we searched for the present species in the molecular line survey of Orion KL performed with the IRAM 30 m telescope. We detected both ^{13}C isotopologues of methyl formate in their first vibrationally excited state. In Sect. 5.1 we summarize the observations, data reduction, and overall results of this survey. We present the new detection in Sect. 5.2. In Sect. 5.3 we explain the assumed model and the excitation and radiative transfer calculations for vibrationally excited ^{13}C and ^{12}C methyl formate. We also compute our obtained ^{12}C/^{13}C ratio and the vibrational temperature for ^{13}C-HCOOCH$_3$ $v_t = 1$.

5.1. Observations, data reduction, and overall results

The molecular line survey towards Orion KL-IRc2 (α(J2000) = $5^h35^m14.5^s$, δ(J2000) = $-5°22'30.0''$) was performed between September 2004 and January 2007 in five observing sessions with the IRAM 30 m telescope. All frequencies allowed by the A, B, C, and D receivers were covered (80−115.5, 130−178, and 197−281 GHz) with a spectral resolution of 1−1.25 MHz. System temperatures, image side-band rejections, and half-power beam widths were in the ranges 100−800 K, 27−13 dB, and 29–9″, from 80 to 281 GHz. The observations were performed in the balanced wobbler-switching mode. Pointing and focus were checked every 1−2 h on nearby quasars. The intensity scale was calibrated with two absorbers at different temperatures using the ATM package (Cernicharo 1985; Pardo et al. 2001).

The data were processed using the GILDAS software[3]. The data reduction consisted of removing lines from the image side-band and fitting and removing baselines. We observed each frequency setting twice, with the second one shifted in frequency by 20 MHz. This allowed us to remove lines from the image side-band down to a level of 30 dB (this means that lines in the image side-band of 30 K will contribute with less than 0.03 K to the final reduced spectrum). Figures are shown in units of main-beam antenna temperature, $T_{MB} = T_A^\star/\eta_{MB}$, where η_{MB} is the main-beam efficiency ranged from 0.82 to 0.48 from the lowest to the highest frequencies. For a detailed description of the observations and data reduction procedures see Tercero et al. (2010).

Up to date, we performed a deep analysis of the data (15 papers have been already published): identifying more than 15 000 spectral features (Tercero et al. 2010; Tercero 2012), detecting new molecules in space (CH_3COOCH_3 and g-CH_3CH_2OCOH in Tercero et al. 2013; NH_3D^+ in Cernicharo et al. 2013; CH_3CH_2SH in Kolesniková et al. 2014; also tentative detections of c-C_6H_5O in Kolesniková et al. 2013 and upper limit calculations for the column density of non detected molecules −cis-CH_2CHCH_2CN and cis-CH_2CHCH_2NC− in Haykal et al. 2013b) and several new isotopologues and

[3] http://www.iram.fr/IRAMFR/GILDAS

Table 2. Torsion-rotation parameters needed for the global fit of transitions involving $v_t = 0$ and $v_t = 1$ torsional energy levels of $^{13}C_2$-methyl formate ($H^{12}COO^{13}CH_3$) provided in this work and comparison with the torsion-rotation parameters obtained in the former global fit of transitions only involving $v_t = 0$ torsional states (Carvajal et al. 2009).

nlm[a]	Operator[b]	Parameter	$v_t = 0, 1$[c]	$v_t = 0$[d]	nlm	Operator	Parameter	$v_t = 0, 1$[c]	$v_t = 0$[d]
220	$(1-\cos 3\gamma)/2$	V_3	369.93168(395)	407.1549(147)[g]	642	$(1-\cos 6\gamma)P^2$	N_v	$-0.312260(869) \times 10^{-3}$	0.0[f]
	P_γ^2	F	5.4785214(464)	5.69168218[e]		$(1-\cos 6\gamma)P_a^2$	K_2	$0.84669(480) \times 10^{-3}$	0.0[f]
211	$P_\gamma P_a$	ρ	0.084337567(345)	0.0845207(106)		$(1-\cos 6\gamma)(P_b^2 - P_c^2)$	c_{11}	$-0.161265(889) \times 10^{-3}$	0.0[f]
202	P_a^2	A^{RAM}	0.58658923(178)	0.5857484(245)		$(1-\cos 6\gamma)(P_aP_b + P_bP_a)$	dd_{ab}	$-0.29738(147) \times 10^{-3}$	0.0[f]
	P_b^2	B^{RAM}	0.29682136(198)	0.2959971(182)		$P_\gamma^4 P^2$	M_v	$0.7960(365) \times 10^{-8}$	0.0[f]
	P_c^2	C^{RAM}	0.173496850(137)	0.1729010(134)		$2\,P_\gamma^4(P_b^2 - P_c^2)$	c_3	$0.13176(197) \times 10^{-7}$	0.0[f]
	$(P_aP_b + P_bP_a)$	D_{ab}	−0.15976497(192)	−0.1573691(747)	624	$(1-\cos 3\gamma)P^4$	f_v	$0.91080(149) \times 10^{-8}$	0.0[f]
440	$(1-\cos 6\gamma)/2$	V_6	25.40353(193)	0.0[f]		$(1-\cos 3\gamma)P_a^2P^2$	k_{5J}	$0.4484(183) \times 10^{-7}$	0.0[f]
422	$P_\gamma^2 P^2$	G_v	$0.27105(240) \times 10^{-5}$	$0.4682(101) \times 10^{-4}$		$(1-\cos 3\gamma)P_a^4$	k_{5K}	$-0.21242(275) \times 10^{-6}$	0.0[f]
	$2P_\gamma^2(P_b^2 - P_c^2)$	c_1	$0.10489(207) \times 10^{-5}$	0.0[f]		$(1-\cos 3\gamma)(P_aP_b + P_bP_a)P^2$	d_{abJ}	$0.46277(344) \times 10^{-7}$	$0.9060(708) \times 10^{-7}$
	$\sin 3\gamma(P_aP_c + P_cP_a)$	D_{ac}	0.0[f]	−0.0040623(839)		$(1-\cos 3\gamma)(P_a^3P_b + P_bP_a^3)$	d_{abK}	$-0.83350(642) \times 10^{-7}$	$0.3349(260) \times 10^{-6}$
	$\sin 3\gamma(P_bP_c + P_cP_b)$	D_{bc}	0.00074120(917)	0.0010563(383)		$(1-\cos 3\gamma)\{P_a^2, (P_b^2 - P_c^2)\}$	c_{2K}	$0.47452(372) \times 10^{-7}$	0.0[f]
	$(1-\cos 3\gamma)P^2$	F_v	−0.00229820(140)	−0.0007557(425)		$P_\gamma^2 P_a^2 P^2$	k_{2J}	$0.4462(154) \times 10^{-9}$	0.0[f]
	$(1-\cos 3\gamma)P_a^2$	k_5	0.01046256(804)	0.0124250(566)		$2P_\gamma^2\{P_a^2, (P_b^2 - P_c^2)\}$	c_{1K}	$0.18733(536) \times 10^{-9}$	0.0[f]
	$(1-\cos 3\gamma)(P_b^2 - P_c^2)$	c_2	$-0.3062(148) \times 10^{-4}$	0.0[f]		$\sin 3\gamma(P_bP_c + P_cP_b)P^2$	D_{bcJ}	$-0.12682(268) \times 10^{-7}$	0.0[f]
	$P_\gamma^2 P_a^2$	k_2	$-0.43892(170) \times 10^{-4}$	0.0[f]	606	P^6	H_J	$-0.755(12) \times 10^{-12}$	$-0.31(1) \times 10^{-13}$
	$(1-\cos 3\gamma)(P_aP_b + P_bP_a)$	d_{ab}	−0.00573380(154)	−0.013852(236)		$P^4P_a^2$	H_{JK}	$0.10555(83) \times 10^{-10}$	0.0[f]
	$P_\gamma^2(P_aP_b + P_bP_a)$	Δ_{ab}	0.0[f]	$-0.16792(565) \times 10^{-3}$		$P^2P_a^4$	H_{KJ}	$-0.34983(244) \times 10^{-10}$	0.0[f]
413	$P_\gamma P_a P^2$	L_v	$0.1824(134) \times 10^{-6}$	$-0.2045(247) \times 10^{-5}$		P_a^6	H_K	$0.50362(252) \times 10^{-10}$	0.0[f]
	$P_\gamma P_a^3$	k_1	$0.127972(329) \times 10^{-4}$	0.0[f]		$2P^4(P_b^2 - P_c^2)$	h_J	$-0.364(6) \times 10^{-12}$	0.0[f]
	$P_\gamma\{P_a, (P_b^2 - P_c^2)\}$	c_4	$0.94726(730) \times 10^{-6}$	$0.39452(688) \times 10^{-5}$		$P^2\{P_a^2, (P_b^2 - P_c^2)\}$	h_{JK}	$0.1996(22) \times 10^{-11}$	$0.1130(25) \times 10^{-11}$
	$P_\gamma\{P_a^2, P_b\}$	δ_{ab}	$-0.343262(938) \times 10^{-5}$	$0.1707(107) \times 10^{-4}$		$\{P_a^4, (P_b^2 - P_c^2)\}$	h_K	$-0.1811(68) \times 10^{-11}$	0.0[f]
404	$-P^4$	Δ_J	$0.24016(201) \times 10^{-6}$	$0.15312(163) \times 10^{-6}$		$P^4(P_aP_b + P_bP_a)$	D_{abJJ}	$0.2077(52) \times 10^{-11}$	0.0[f]
	$-P^2P_a^2$	Δ_{JK}	$-0.235426(785) \times 10^{-5}$	$0.21223(170) \times 10^{-5}$		$P^2(P_a^3P_b + P_bP_a^3)$	D_{abJK}	$-0.10787(148) \times 10^{-10}$	0.0[f]
	$-P_a^4$	Δ_K	$0.576749(422) \times 10^{-5}$	$-0.17369(181) \times 10^{-5}$	615	$P_\gamma P_a P^4$	l_v	$0.14903(534) \times 10^{-10}$	0.0[f]
	$-2P^2(P_b^2 - P_c^2)$	δ_J	$0.8245(100) \times 10^{-7}$	$0.39739(813) \times 10^{-7}$					
	$-\{P_a^2, (P_b^2 - P_c^2)\}$	δ_K	$-0.41365(637) \times 10^{-7}$	$0.108794(621) \times 10^{-5}$					
	$P^2(P_aP_b + P_bP_a)$	D_{abJ}	$-0.48884(361) \times 10^{-6}$	$0.24287(221) \times 10^{-6}$					
	$(P_a^3P_b + P_bP_a^3)$	D_{abK}	$0.1345545(843) \times 10^{-5}$	$0.13608(491) \times 10^{-5}$					

Notes. [a] Notation from Ilyushin et al. (2003); $n = l + m$, where n is the total order of the operator, l is the order of the torsional part and m is the order of the rotational part. [b] Notation from Ilyushin et al. (2003). $\{A, B\} = AB + BA$. The product of the parameter and operator from a given row yields the term actually used in the vibration-rotation-torsion Hamiltonian, except for F, ρ and A, which occur in the Hamiltonian in the form $F(P_\gamma - \rho P_a)^2 + A^{\mathrm{RAM}}P_a^2$. [c] Values of the parameters from the present fit, for the ground torsional state $v_t = 0$ and the first excited torsional state $v_t = 1$. All parameter values are in cm^{-1} except for ρ which is unitless. Statistical uncertainties are given in parentheses in units of the last quoted digit. [d] Values of the parameters from the fit for the ground torsional state $v_t = 0$ given by Carvajal et al. (2009). The 27 parameters were fitted for 936 MW lines from $v_t = 0$ with a root mean square of 97 kHz. All parameter values are in cm^{-1} except for ρ which is unitless. Statistical uncertainties are given in parentheses in units of the last quoted digit. [e] The internal rotation constant F of $HCOO^{13}CH_3$ was kept fixed to the ab initio value calculated in the equilibrium structure (see Carvajal et al. 2009). [f] Kept fixed. [g] Very large effective value obtained as a consequence of fixing F parameter to a large ab initio value and because F, V_3 and V_6 were not able to fit them at the same time only from the ground torsional state (Carvajal et al. 2009).

Table 3. Rotational constants in the principal axis system (PAM), angles between the principal axis and the methyl top axis, and internal rotation parameters upon isotopic substitution.

	$HCOOCH_3$[a] Global fit (v_t = 0, 1)	$HCOO^{13}CH_3$[b] Global fit (v_t = 0)	$HCOO^{13}CH_3$[c] Global fit (v_t = 0, 1)
A(MHz)	19 924.4249(433)	19 629.65(176)	19 707.8000(625)
B(MHz)	6947.9458(414)	6804.42(171)	6776.1833(660)
C(MHz)	5318.10685(450)	5183.442(402)	5201.30471(410)
$<(i,a)$[d]	53.06	51.68	52.18(25)
θ_{RAM}[e]	24.87951(13)	23.68	23.89824(22)
ρ	0.08427227(25)	0.0845207(106)	0.084337567(345)
F (cm^{-1})	5.497592(59)	5.69168218[f]	5.4785214(464)
V_3 (cm^{-1})	370.7398(58)	407.1549(147)	369.93168(395)
σ[g]	0.67	1.08	0.77
Nº of transitions	15 840	936	9455
Nº of fitted parameters	53	27	52

Notes. [(a)] Rotation-torsion parameters for the normal species $HCOOCH_3$ obtained in Tudorie et al. (2012) with the RAM-axis system, after transforming the RAM values for the A, B, C rotational parameters into PAM values following the procedure described in Carvajal et al. (2007). The RAM to PAM transformation is given in Carvajal et al. (2010). [(b)] Rotation-torsion parameters for $^{13}C_2$-methyl formate from Carvajal et al. (2009) transformed to the principal axis system. [(c)] Rotation-torsion parameters for $^{13}C_2$-methyl formate from the present work transformed into the principal axis system. [(d)] Angle in degrees between the a-principal axis and the methyl top axis (i). [(e)] The angle θ_{RAM} between the a-principal axis and the a-RAM axis is given in degrees and obtained from Eq. (1) from Carvajal et al. (2007), with the parameters A^{RAM}, B^{RAM}, C^{RAM}, and D_{ab} of Table 2. [(f)] Fixed to the ab initio value (Carvajal et al. 2009). [(g)] Unitless standard deviation.

Table 4. Kinematic parameters and physical conditions of the Orion-KL spatial components.

Parameter	Extended ridge (ER)	Compact ridge (CR)	Plateau (P)	Hot core (HC)
Source diameter (″)	≃120 (120)	5–15 (15)	20–30 (30)	5–10 (10)
Offset (from IRc2) (″)	0 (0)	7 (7)	0 (0)	2–3 (2)
$n(H_2)$ (cm^{-3})	$\simeq 10^5$	$\simeq 10^6$	$\simeq 10^6$	10^7–10^8
T_k (K)	≃60 (60)	80–150 (110)	100–150 (125)	150–300 (225)
Δv_{FWHM} ($km\,s^{-1}$)	≃4 (4)	3–5 (4)	≃25 (25)	5–15 (10)
v_{LSR} ($km\,s^{-1}$)	8–10 (8)	7–9 (7.5)	6–11 (9)	3–6 (5.5)

Notes. Parameters compiled from different authors: Blake et al. (1987); Schilke et al. (2001); Persson et al. (2007); Tercero et al. (2010); Neill et al. (2013). The values between parenthesis are those adopted for the model of $HCOOCH_3$ v_t = 1 and ^{13}C-$HCOOCH_3$ v_t = 0.

vibrationally excited states of well-known molecules in this source (^{13}C-CH_3CH_2CN in Demyk et al. 2007; ^{13}C-$HCOOCH_3$ in Carvajal et al. 2009; $CH_3CH_2{}^{15}N$, CH_3CHDCN, and CH_2DCH_2CN in Margulès et al. 2009; $DCOOCH_3$ in Margulès et al. 2010; ^{18}O-$HCOOCH_3$ in Tercero et al. 2012; NH_2CHO ν_{12} = 1 in Motiyenko et al. 2012; CH_3CH_2CN ν_{10} = 1 and ν_{12} = 1 in Daly et al. 2013; $HCOOCH_2D$ in Coudert et al. 2013; CH_2CHCN $\nu_{10} = 1 \Leftrightarrow (\nu_{11} = 1, \nu_{15} = 1)$ in López et al. 2014), and constraining physical and chemical parameters by means of the analysis of different families of molecules (OCS, CS, H_2CS, HCS^+, CCS, CCCS species in Tercero et al. 2010; SiO and SiS species in Tercero et al. 2011; CH_3CH_2CN species in Daly et al. 2013; SO and SO_2 species in Esplugues et al. 2013a; HC_3N and HC_5N species in Esplugues et al. 2013b; CH_3CN in Bell et al. 2014; CH_2CHCN species and the isocyanides in López et al. 2014). In addition and to analyze some of these results, we modelese the following molecules: CH_3SH, CH_3OH, CH_3CH_2OH in Kolesniková et al. (2014), $HCOOCH_3$ in Margulès et al. (2010), and NH_2CHO in Motiyenko et al. (2012). Nevertheless, the study of this line survey is still open and several groups are working simultaneously based on the scope of these observations[4].

In agreement with numerous works of this region (see e.g. Blake et al. 1987; Schilke et al. 2001; Persson et al. 2007; Neill et al. 2013), at least four cloud components could be identified in the line profiles of our low-resolution spectral lines, which are characterized by different radial velocities and line widths (Tercero et al. 2010, 2011). Each component corresponds to specific region of the cloud that overlaps in our telescope beam. Table 4 summarizes the kinematic and physical parameters of the different components in Orion-KL.

5.2. Results

The two ^{13}C isotopologues of $HCOOCH_3$ in their first vibrationally excited state (v_t = 1) have been detected in Orion-KL by means of 135 spectral features (77 of them practically unblended) without missing transitions in the range 80–280 GHz. Figure 2 shows selected detected lines of the two isotopologues together with our best model (see below). The black histogram line corresponds with the observed spectra. The model of the $H^{13}COOCH_3$ v_t = 1 and $HCOO^{13}CH_3$ ν_t = 1 lines is shown in red and dark blue, respectively. In all boxes unblended or slightly blended detected lines of these species are depicted. The cyan blue line represents the total model compiled from our already published work (see Sect. 5.1). In Table 5 we list all detected features in our line survey. These detections are based on an inspection of the data and the modelled synthetic spectrum of the studied species and all the species already identified in our previous papers (see above). The observed main-beam temperature and the radial velocity where obtained from the peak channel of our spectra, therefore, errors in the baselines −up to ±0.15 K for spectra at 1.3 mm due to the extremely high line density (line confusion limit) − and contribution from other species might affect the T_{mb}^{obs} value. Adding species to our total model allows reducing the uncertainty in the baselines, so, in general, the T_{mb}^{obs}

[4] The data of the IRAM 30 m line survey of Orion KL are available in ascii format on request to B. Tercero.

Table 5. Detected lines of ^{13}C-HCOOCH$_3$ $v_t = 1$ towards Orion KL.

Spec.	J	K_a	K_c	p	J'	K'_a	K'_c	p'	Calc. freq. (MHz)	E_u (K)	$S_{ij}\mu^2$ (D^2)	Obs. freq. (MHz)	v_{LSR} (km s^{-1})	T_{mb}^{obs} (K)	T_{mb}^{mod} (K)	Blend
A-^{13}C$_1$	12	1	12	+	11	1	11	+	130 348.229	229.4	32.1	130 349.3	4.6 ± 1.2	0.06	0.03	
E-^{13}C$_1$	12	–1	12		11	–1	11		130 424.730	229.5	32.2	130 424.3	8.1 ± 1.2	0.04	0.03	
A-^{13}C$_2$	11	3	9	+	10	3	8	+	130 674.060	231.2	26.8	130 673.6	8.0 ± 1.1	0.07	0.03	CH$_3$CH$_2$C^{15}N
E-^{13}C$_2$	11	5	6		10	5	5		131 497.371	340.9	23.2	131 497.9	5.7 ± 1.1	0.03	0.02	
E-^{13}C$_2$	11	–3	9		10	–3	8		131 600.450	329.8	26.6	131 600.6	6.6 ± 1.1	0.03	0.02	
A-^{13}C$_2$	11	4	8	–	10	4	7	–	131 626.157	235.9	25.2	131 626.6	6.0 ± 1.1	0.07	0.02	(CH$_3$)$_2$CO
A-^{13}C$_2$	11	4	7	+	10	4	6	+	132 401.079	236.0	25.2	132 400.5	8.3 ± 1.1	0.04	0.02	CH$_3$CHDCN
A-^{13}C$_1$	11	3	9	+	10	3	8	+	132 807.823	231.8	27.4	132 806.7	9.6 ± 1.1	0.07	0.03	
A-^{13}C$_1$	11	9	2	–	10	9	1	–	132 945.107	279.3	9.86	132 946.6	3.7 ± 1.1	0.07	0.02	CCCS
A-^{13}C$_1$	11	9	3	+	10	9	2	+	132 945.107	279.3	9.86	†	3.7 ± 1.1			
E-^{13}C$_2$	11	3	8		10	3	7		136 042.486	330.6	26.8	136 042.9	6.2 ± 1.1	0.03	0.03	
E-^{13}C$_1$	11	3	8		10	3	7		138 640.538	232.8	27.6	138 640.6	6.9 ± 1.1	0.04	0.03	
A-^{13}C$_2$	13	1	13	+	12	1	12	+	138 830.565	235.5	34.0	138 829.7	8.9 ± 1.1	0.06	0.04	
E-^{13}C$_1$	12	–2	11		11	–2	10		139 241.862	234.5	31.5	139 239.2	12.6 ± 1.1	0.06	0.03	CH$_2$DCH$_2$CN
E-^{13}C$_1$	13	–1	13		12	–1	12		140 917.742	236.2	35.0	140 918.6	5.3 ± 1.1	0.04	0.04	
A-^{13}C$_1$	13	0	13	+	12	0	12	+	140 937.135	236.2	34.8	140 937.6	6.1 ± 1.1	0.13	0.04	CH$_2$DOH
E-^{13}C$_1$	13	0	13		12	0	12		141 008.471	236.2	35.0	141 007.8	8.3 ± 1.1	0.09	0.04	
E-^{13}C$_1$	12	1	11		11	1	10		141 542.530	234.2	31.6	141 543.0	6.1 ± 1.1	0.05	0.04	
A-^{13}C$_2$	12	3	10	+	11	3	9	+	142 240.894	238.0	29.5	142 240.3	8.2 ± 1.1	0.04	0.03	
E-^{13}C$_2$	12	4	8		11	4	7		144 894.428	341.8	28.2	144 895.6	4.6 ± 1.0	0.06	0.03	
E-^{13}C$_2$	12	–4	9		11	–4	8		144 984.322	341.4	28.2	144 983.7	8.4 ± 1.0	0.05	0.03	
E-^{13}C$_1$	12	7	5		11	7	4		145 262.992	266.0	21.5	145 262.9	7.1 ± 1.0	0.07	0.02	U
A-^{13}C$_1$	12	7	6	+	11	7	5	+	145 282.393	265.1	21.5	145 282.9	5.9 ± 1.0	0.07	0.04	
A-^{13}C$_1$	12	7	5	–	11	7	4	–	145 282.519	265.1	21.5	†	6.2 ± 1.0			
E-^{13}C$_1$	12	5	7		11	5	6		146 170.669	250.0	27.0	146 170.3	7.7 ± 1.0	0.15	0.03	H^{13}COOCH$_3$
E-^{13}C$_1$	12	4	8		11	4	7		147 500.782	244.1	28.9	147 501.6	5.4 ± 1.0	0.15	0.07	
E-^{13}C$_1$	12	–4	9		11	–4	8		147 501.246	243.7	28.7	†	6.3 ± 1.0			
A-^{13}C$_1$	13	2	12	–	12	2	11	–	149 734.053	241.5	34.0	149 734.5	6.0 ± 1.0	0.05	0.04	
A-^{13}C$_1$	12	2	10	+	11	2	9	+	150 951.028	237.3	31.4	150 950.6	7.9 ± 1.0	0.04	0.04	
E-^{13}C$_1$	14	0	14		13	–1	13		151 328.687	243.5	6.07	151 331.6	1.3 ± 1.0	0.11	0.05	U
A-^{13}C$_1$	14	1	14	+	13	1	13	+	151 329.124	243.4	37.5	†	2.2 ± 1.0			
E-^{13}C$_1$	14	0	14		13	0	13		151 452.158	243.5	37.7	151 451.6	8.1 ± 1.0	0.04	0.05	
E-^{13}C$_2$	13	–3	11		12	–3	10		154 267.593	344.1	32.4	154 267.7	6.8 ± 1.0	0.08	0.04	CH$_3$CHO
A-^{13}C$_2$	13	7	7	+	12	7	6	+	154 902.510	272.0	24.4	154 902.4	7.2 ± 1.0	0.24	0.05	SO$_2$ $\nu_2 = 1$
A-^{13}C$_2$	13	7	6	–	12	7	5	–	154 902.822	272.0	24.4	†	7.8 ± 1.0			
A-^{13}C$_1$	13	3	11	+	12	3	10	+	156 106.621	246.2	33.2	156 107.9	4.6 ± 1.0	0.15	0.04	HCOOCH$_3$ $\nu_t = 1$
E-^{13}C$_1$	13	–3	11		12	–3	10		156 705.635	246.5	33.3	156 705.5	7.3 ± 1.0	0.11	0.04	CH$_3$CH$_2$C^{15}N
E-^{13}C$_1$	13	10	3		12	10	2		156 879.965	307.6	14.4	156 880.5	6.0 ± 1.0	0.05	0.01	
E-^{13}C$_1$	13	9	4		12	9	3		157 026.174	294.9	18.4	157 026.5	6.4 ± 1.0	0.09	0.02	HCOOCH$_3$

Notes. Emission lines of ^{13}C-HCOOCH$_3$ $v_t = 1$ present in the spectral scan of Orion-KL from the IRAM 30-m radio-telescope. Column (1) indicates the species, being A-^{13}C$_1$: A-H^{13}COOCH$_3$ $v_t = 1$, E-^{13}C$_1$: E-H^{13}COOCH$_3$ $v_t = 1$, A-^{13}C$_2$: A-HCOO^{13}CH$_3$ $v_t = 1$, and E-^{13}C$_2$: E-HCOO^{13}CH$_3$ $v_t = 1$, Cols. (2)–(9) indicate the line transition, Col. (10) gives the predicted frequency obtained with the Hamiltonian parameters of this work for ^{13}C$_2$-MF and from Carvajal et al. (2010) for ^{13}C$_1$-MF, Col. (11) upper level energy, Col. (12) line strength, Col. (13) observed frequency assuming a v_{LSR} of 7 km s^{-1}, Col. (14) the radial velocity, Col. (15) observed main-beam temperature, Col. (16) modelled main-beam temperature, and Col. (17) blends. † Blended with previous line.

Table 5. continued.

Spec.	J	K_a	K_c	p	J'	K'_a	K'_c	p'	Calc. freq. (MHz)	E_u (K)	$S_{ij}\mu^2$ (D^2)	Obs. freq. (MHz)	v_{LSR} ($km\,s^{-1}$)	T_{mb}^{obs} (K)	T_{mb}^{mod} (K)	Blend
A-$^{13}C_1$	13	10	4	–	12	10	3	–	157 221.146	306.4	14.4	157 224.1	1.4 ± 1.0	0.15	0.05	U
A-$^{13}C_1$	13	10	3	+	12	10	2	+	157 221.146	306.4	14.4	†	1.4 ± 1.0			
E-$^{13}C_1$	13	8	5		12	8	4		157 227.514	283.6	22.0	†	13.6 ± 1.0		0.02	
E-$^{13}C_2$	13	–4	10		12	–4	9		157 232.535	348.9	30.8	157 231.6	8.9 ± 1.0	0.11	0.04	CH_3OH
A-$^{13}C_2$	13	4	9	+	12	4	8	+	158 076.398	250.5	31.1	158 076.5	6.9 ± 0.9	0.10	0.04	
A-$^{13}C_1$	13	5	9	+	12	5	8	+	158 310.862	257.0	30.0	158 311.6	5.7 ± 0.9	0.14	0.04	$^{13}CH_3OH$
E-$^{13}C_2$	14	–2	13		13	–2	12		158 376.417	346.9	36.1	158 376.5	6.8 ± 0.9	0.07	0.05	
E-$^{13}C_1$	13	–6	8		12	–6	7		158 492.862	264.3	27.8	158 492.8	7.1 ± 0.9	0.13	0.03	U
E-$^{13}C_1$	13	–5	9		12	–5	8		159 175.181	257.1	30.1	159 175.2	6.9 ± 0.9	0.10	0.04	CH_3CH_2OCOH
E-$^{13}C_2$	14	1	13		13	1	12		159 621.190	346.8	36.1	159 620.4	8.4 ± 0.9	0.06	0.05	CH_3CH_2OCOH
E-$^{13}C_1$	13	–4	10		12	–4	9		159 907.354	251.3	31.4	159 906.5	8.6 ± 0.9	0.10	0.04	U
E-$^{13}C_1$	13	3	10		12	3	9		165 795.305	248.1	33.6	165 796.4	5.1 ± 0.9	0.15	0.05	$CH_3C^{13}CH$
A-$^{13}C_2$	14	10	4	+	13	10	3	+	166 582.134	313.8	18.1	166 581.5	8.2 ± 0.9	0.08	0.04	
A-$^{13}C_2$	14	10	5	–	13	10	4	–	166 582.134	313.8	18.1	†	8.2 ± 0.9			
E-$^{13}C_2$	14	8	6		13	8	5		166 627.702	389.3	25.0	166 627.5	7.4 ± 0.9	0.08	0.03	
A-$^{13}C_2$	14	6	9	–	13	6	8	–	167 331.309	271.4	30.3	167 330.3	8.9 ± 0.9	0.12	0.04	U
A-$^{13}C_2$	14	6	8	+	13	6	7	+	167 355.684	271.4	30.3	167 356.5	5.6 ± 0.9	0.10	0.04	
E-$^{13}C_1$	14	–3	12		13	–3	11		168 050.461	254.5	36.1	168 050.1	7.7 ± 0.9	0.07	0.05	
A-$^{13}C_2$	14	5	9	–	13	5	8	–	168 269.790	264.3	32.1	168 270.3	6.1 ± 0.9	0.16	0.04	$HCOO^{13}CH_3$
A-$^{13}C_1$	14	7	8	+	13	7	7	+	169 803.580	280.8	28.4	169 802.4	9.1 ± 0.9	0.14	0.06	U
A-$^{13}C_1$	14	7	7	–	13	7	6	–	169 804.698	280.8	28.4	†	11.1 ± 0.9			
A-$^{13}C_2$	16	0	16	+	15	0	15	+	169 839.735	258.4	41.7	169 839.4	7.6 ± 0.9	0.22	0.06	$CH_3^{13}CH_2CN$
E-$^{13}C_2$	16	–1	16		15	–1	15		169 881.101	356.9	42.0	169 880.5	8.1 ± 0.9	0.10	0.06	
E-$^{13}C_2$	14	2	12		13	2	11		171 156.971	351.0	35.9	171 157.6	5.9 ± 0.9	0.05	0.06	
E-$^{13}C_2$	18	–2	17		17	–2	16		200 012.238	382.3	46.5	200 011.0	8.9 ± 0.7	0.11	0.08	
E-$^{13}C_2$	16	3	13		15	3	12		200 350.331	372.6	40.9	200 351.0	5.9 ± 0.7	0.08	0.07	
E-$^{13}C_1$	17	–3	15		16	–3	14		201 246.113	281.9	44.4	201 244.8	8.9 ± 0.7	0.21	0.08	CH_3CH_2OH
A-$^{13}C_1$	16	4	12	+	15	4	11	+	202 078.548	278.5	40.7	202 078.1	7.7 ± 0.7	0.33	0.07	U
A-$^{13}C_2$	17	11	7	+	16	11	6	+	202 460.334	355.2	26.1	202 460.6	6.7 ± 0.7	0.15	0.06	
A-$^{13}C_2$	17	11	6	–	16	11	5	–	202 460.334	355.2	26.1	†	6.7 ± 0.7			
E-$^{13}C_1$	16	4	12		15	4	11		202 695.684	279.0	44.4	202 695.6	7.1 ± 0.7	0.25	0.08	U
A-$^{13}C_2$	17	9	8	–	16	9	7	–	202 701.664	328.6	32.4	202 701.7	6.9 ± 0.7	0.16	0.09	
A-$^{13}C_2$	17	9	9	+	16	9	8	+	202 701.650	328.6	32.4	†	6.9 ± 0.7			
A-$^{13}C_1$	18	1	17	–	17	1	16	–	202 854.699	285.1	47.6	202 854.4	7.5 ± 0.7	0.14	0.08	
E-$^{13}C_1$	18	1	17		17	1	16		203 103.686	285.3	47.8	203 099.3	13.5 ± 0.7	0.04	0.09	$DCOOCH_3$
A-$^{13}C_2$	17	4	14	–	16	4	13	–	203 145.664	285.9	42.2	203 146.8	5.3 ± 0.7	0.25	0.07	$SO^{17}O$ $HCCC^{15}N$
A-$^{13}C_1$	19	1	19	+	18	1	18	+	203 678.875	287.3	51.0	203 679.3	6.4 ± 0.7	0.16	0.09	U
A-$^{13}C_1$	19	0	19	+	18	0	18	+	203 682.196	287.3	51.0	203 683.2	5.6 ± 0.7	0.10	0.09	
E-$^{13}C_1$	19	–1	19		18	–1	18		203 734.744	287.4	51.3	203 733.1	9.5 ± 0.7	0.14	0.09	U
E-$^{13}C_1$	19	0	19		18	0	18		203 737.849	287.4	51.3	†	14.0 ± 0.7		0.09	
A-$^{13}C_1$	17	2	15	+	16	2	14	+	203 884.346	281.3	44.4	203 884.2	7.2 ± 0.7	0.23	0.08	$HCOOCH_3$ $\nu_t = 1$

Table 5. continued.

Spec.	J	K_a	K_c	p	J'	K'_a	K'_c	p'	Calc. freq. (MHz)	E_u (K)	$S_{ij}\mu^2$ (D^2)	Obs. freq. (MHz)	v_{LSR} (km s^{-1})	T_{mb}^{obs} (K)	T_{mb}^{mod} (K)	Blend
																$H^{13}COOCH_3$
A-$^{13}C_2$	17	6	12	–	16	6	11	–	204 024.731	299.0	39.3	204 024.3	7.6 ± 0.7	0.09	0.06	CH_3COOCH_3
A-$^{13}C_1$	17	10	8	–	16	10	7	–	205 972.338	342.4	30.3	205 972.2	7.2 ± 0.7	0.39	0.12	H_2CS
A-$^{13}C_1$	17	10	7	+	16	10	6	+	205 972.338	342.4	30.3	†	7.2 ± 0.7			
A-$^{13}C_1$	17	7	11	+	16	7	10	+	206 865.964	308.8	38.3	206 867.3	5.1 ± 0.7	0.04	0.06	CH_3COOCH_3
A-$^{13}C_1$	17	6	12	–	16	6	11	–	207 553.192	300.4	40.4	207 553.6	6.5 ± 0.7	0.14	0.07	U
A-$^{13}C_2$	19	2	18	–	18	2	17	–	210 097.941	293.7	48.9	210 097.2	8.0 ± 0.7	0.18	0.09	
E-$^{13}C_2$	19	–2	18		18	–2	17		210 345.827	392.4	49.2	210 346.0	6.8 ± 0.7	0.18	0.09	
A-$^{13}C_2$	20	0	20	+	19	1	19	+	211 082.205	296.0	8.83	211 087.2	0.0 ± 0.7	0.19	0.10	
A-$^{13}C_2$	20	1	20	+	19	1	19	+	211 085.095	296.0	52.3	†	4.1 ± 0.7			
A-$^{13}C_2$	20	0	20	+	19	0	19	+	211 087.344	296.0	52.3	†	7.3 ± 0.7			
A-$^{13}C_2$	20	1	20	+	19	0	19	+	211 090.234	296.0	8.83	†	11.4 ± 0.7			
E-$^{13}C_2$	20	0	20		19	–1	19		211 134.083	394.5	8.60	211 137.3	2.4 ± 0.7	0.24	0.09	NH_2CHO
E-$^{13}C_2$	20	–1	20		19	–1	19		211 136.716	394.5	52.6	†	6.1 ± 0.7			
A-$^{13}C_2$	17	3	14	–	16	3	13	–	211 372.277	284.0	43.3	211 376.0	1.8 ± 0.7	0.16	0.08	$CH_2CH^{13}CN$/U
E-$^{13}C_2$	18	2	16		17	2	15		211 377.266	388.8	46.0	†	8.8 ± 0.7		0.08	
A-$^{13}C_1$	19	1	18	–	18	1	17	–	213 261.995	295.3	50.2	213 262.2	6.7 ± 0.7	0.13	0.09	
A-$^{13}C_1$	18	2	16	+	17	2	15	+	213 882.009	291.5	47.0	213 884.7	3.2 ± 0.7	0.23	0.09	$^{13}CH_3CH_2CN$
																CH_2CHCN $v_{11} = 2$
E-$^{13}C_1$	20	0	20		19	–1	19		214 193.599	297.6	9.04	214 197.2	1.9 ± 0.7	0.34	0.13	
E-$^{13}C_1$	20	–1	20		19	–1	19		214 195.705	297.6	54.0	†	4.9 ± 0.7			
E-$^{13}C_1$	20	0	20		19	0	19		214 197.429	297.6	54.0	†	7.3 ± 0.7			
E-$^{13}C_1$	20	–1	20		19	0	19		214 199.535	297.6	9.04	†	10.2 ± 0.7			
A-$^{13}C_2$	18	10	9	–	17	10	8	–	214 572.059	351.5	32.9	214 572.2	6.8 ± 0.7	0.27	0.09	$^{13}C^{17}O$
A-$^{13}C_2$	18	10	8	+	17	10	7	+	214 572.060	351.5	32.9	†	6.8 ± 0.7			
E-$^{13}C_1$	17	3	14		16	3	13		215 322.039	286.0	44.6	215 324.7	3.3 ± 0.7	0.11	0.09	U
E-$^{13}C_2$	18	–4	15		17	–4	14		215 326.475	395.1	45.2	†	9.5 ± 0.7		0.08	
E-$^{13}C_2$	18	–6	13		17	–6	12		217 440.211	408.2	42.5	217 441.0	6.0 ± 0.7	0.16	0.07	
A-$^{13}C_1$	18	4	15	–	17	4	14	–	218 060.270	297.8	46.2	218 057.1	11.4 ± 0.7	0.20	0.08	c-C_3H_2
E-$^{13}C_1$	18	8	10		17	8	9		218 648.438	330.1	39.3	218 647.0	8.9 ± 0.7	0.10	0.06	U
E-$^{13}C_1$	18	–9	10		17	–9	9		219 017.617	340.8	36.8	219 017.2	7.6 ± 0.7	0.10	0.06	
A-$^{13}C_2$	19	3	17	+	18	3	16	+	219 092.328	300.8	48.4	219 092.2	7.2 ± 0.7	0.13	0.09	
E-$^{13}C_2$	18	5	13		17	5	12		219 883.920	401.8	43.3	219 885.9	4.3 ± 0.7	0.13	0.08	CH_2CHCN $v_{11} = 2$
																U
E-$^{13}C_1$	19	–3	17		18	–3	16		222 753.709	302.8	49.8	222 753.4	7.5 ± 0.7	0.09	0.09	U
E-$^{13}C_1$	18	5	13		17	5	12		224 161.641	305.0	44.4	224 160.9	7.9 ± 0.7	0.14	0.08	CH_3COOCH_3
E-$^{13}C_2$	18	4	14		17	4	13		225 917.084	397.1	45.7	225 917.1	7.0 ± 0.7	0.14	0.09	
A-$^{13}C_2$	19	10	10	–	18	10	9	–	226 614.150	362.4	36.4	226 614.6	6.4 ± 0.7	0.42	0.10	CH_2CHCN $v_{15} = 1$
A-$^{13}C_2$	19	10	9	+	18	10	8	+	226 614.152	362.4	36.4	†	6.4 ± 0.7			
E-$^{13}C_2$	19	–9	11		18	–9	10		227 459.769	448.7	39.1	227 459.6	7.3 ± 0.7	0.18	0.06	
A-$^{13}C_1$	18	4	14	+	17	4	13	+	229 246.345	299.9	46.5	229 247.1	6.0 ± 0.7	0.24	0.09	CH_3CH_2CN
E-$^{13}C_2$	19	6	13		18	6	12		229 294.250	419.7	45.2	229 294.6	6.5 ± 0.7	0.30	0.08	U
E-$^{13}C_2$	19	–6	14		18	–6	13		229 951.441	419.2	45.2	229 952.1	6.2 ± 0.7	0.11	0.08	

Table 5. continued.

Spec.	J	K_a	K_c	p	J'	K'_a	K'_c	p'	Calc. freq. (MHz)	E_u (K)	$S_{ij}\mu^2$ (D^2)	Obs. freq. (MHz)	v_{LSR} (km s^{-1})	T_{mb}^{obs} (K)	T_{mb}^{mod} (K)	Blend
E-$^{13}C_1$	18	4	14		17	4	13		230 063.581	300.4	46.8	230 064.6	5.7 ± 0.7	0.21	0.10	U
A-$^{13}C_1$	19	14	6	–	18	14	5	–	230 100.629	427.4	23.6	230 100.8	6.8 ± 0.7	0.15	0.14	
A-$^{13}C_1$	19	14	5	+	18	14	4	+	230 100.629	427.4	23.6	†	6.8 ± 0.7			
E-$^{13}C_2$	19	–5	15		18	–5	14		230 101.552	412.2	46.0	†	8.0 ± 0.7			
A-$^{13}C_1$	19	9	11	+	18	9	10	+	230 720.161	351.4	40.1	230 719.6	7.7 ± 0.7	0.15	0.12	
A-$^{13}C_1$	19	9	10	–	18	9	9	–	230 720.299	351.4	40.1	†	7.9 ± 0.7			
A-$^{13}C_2$	22	0	22	+	21	1	21	+	231 708.149	317.7	9.76	231 709.6	5.2 ± 0.6	0.22	0.21	
A-$^{13}C_2$	22	1	22	+	21	1	21	+	231 709.053	317.7	57.7	†	6.3 ± 0.6			
A-$^{13}C_2$	22	0	22	+	21	0	21	+	231 709.768	317.7	57.7	†	7.3 ± 0.6			
A-$^{13}C_2$	22	1	22	+	21	0	21	+	231 710.673	317.7	9.76	†	8.4 ± 0.6			
A-$^{13}C_1$	20	2	18	+	19	2	17	+	234 053.346	313.5	52.3	234 054.0	6.2 ± 0.6	0.29	0.10	
E-$^{13}C_1$	22	0	22		21	–1	21		235 113.385	319.7	10.0	235 114.0	6.2 ± 0.6	0.35	0.24	
E-$^{13}C_1$	22	–1	22		21	–1	21		235 114.014	319.7	59.4	†	7.0 ± 0.6			
E-$^{13}C_1$	22	0	22		21	0	21		235 114.538	319.7	59.4	†	7.7 ± 0.6			
E-$^{13}C_1$	22	–1	22		21	0	21		235 115.167	319.7	10.0	†	8.5 ± 0.6			
E-$^{13}C_2$	20	–8	13		19	–8	12		240 214.055	449.0	44.6	240 213.9	7.2 ± 0.6	0.24	0.07	
A-$^{13}C_2$	22	1	21	–	21	1	20	–	241 080.593	327.0	56.9	241 082.0	5.2 ± 0.6	0.24	0.10	
E-$^{13}C_1$	20	–4	17		19	–4	16		241 374.048	320.9	51.9	241 373.5	7.7 ± 0.6	0.12	0.10	CH_3CH_2OCOH
E-$^{13}C_1$	22	–2	21		21	–2	20		244 776.097	329.3	58.6	244 774.9	8.5 ± 0.6	0.21	0.11	
E-$^{13}C_1$	22	1	21		21	1	20		244 800.362	329.3	58.6	244 799.9	7.5 ± 0.6	0.68	0.21	$CH_3CH_2^{13}CN$ $H^{13}COOCH_3$
A-$^{13}C_2$	21	9	13	+	20	9	12	+	251 115.944	373.3	45.4	251 115.9	7.1 ± 0.6	0.13	0.13	
A-$^{13}C_2$	21	9	12	–	20	9	11	–	251 116.550	373.3	45.4	†	7.8 ± 0.6			
A-$^{13}C_2$	24	0	24	+	23	1	23	+	252 327.721	341.5	10.7	252 327.2	7.6 ± 0.6	0.44	0.26	
A-$^{13}C_2$	24	1	24	+	23	0	23	+	252 328.505	341.5	10.7	†	8.5 ± 0.6			
A-$^{13}C_2$	24	1	24	+	23	1	23	+	252 328.001	341.5	63.0	†	7.9 ± 0.6			
A-$^{13}C_2$	24	0	24	+	23	0	23	+	252 328.225	341.5	63.0	†	8.2 ± 0.6			
A-$^{13}C_2$	21	7	14	–	20	7	13	–	252 689.210	352.5	49.4	252 689.8	6.3 ± 0.6	0.18	0.08	
E-$^{13}C_2$	21	7	14		20	7	13		252 703.017	451.8	49.4	252 704.8	4.8 ± 0.6	0.14	0.08	CH_3COOCH_3
A-$^{13}C_2$	21	6	16	–	20	6	15	–	253 342.936	344.1	51.0	253 343.5	6.4 ± 0.6	0.15	0.09	
A-$^{13}C_1$	21	14	8	–	20	14	7	–	254 444.432	451.2	25.5	254 444.7	6.7 ± 0.6	0.15	0.07	
A-$^{13}C_1$	21	14	7	+	20	14	6	+	254 444.432	451.2	25.5	†	6.7 ± 0.6			
A-$^{13}C_1$	21	14	7	+	20	14	7	–	254 444.432	451.2	6.22	†	6.7 ± 0.6			
A-$^{13}C_1$	21	14	8	–	20	14	6	+	254 444.432	451.2	6.22	†	6.7 ± 0.6			
E-$^{13}C_1$	21	10	11		20	10	10		254 626.092	388.9	44.1	254 625.8	7.4 ± 0.6	0.22	0.06	
E-$^{13}C_1$	22	2	20		21	2	19		254 899.597	337.9	58.0	254 899.8	6.8 ± 0.6	0.15	0.11	
A-$^{13}C_1$	21	9	13	+	20	9	12	+	255 417.206	375.3	46.5	255 417.1	7.1 ± 0.6	0.07	0.14	
A-$^{13}C_1$	11	5	7	+	10	4	6	+	255 417.848	242.4	2.44	†	7.9 ± 0.6			
A-$^{13}C_1$	21	9	12	–	20	9	11	–	255 418.028	375.3	46.5	†	8.1 ± 0.6			
A-$^{13}C_2$	21	5	16	–	20	5	15	–	261 016.105	338.3	52.3	261 016.8	6.2 ± 0.6	0.43	0.10	
A-$^{13}C_2$	22	12	10	+	21	12	9	+	262 404.906	427.7	40.9	262 404.6	7.3 ± 0.6	0.18	0.10	
A-$^{13}C_2$	22	12	11	–	21	12	10	–	262 404.906	427.7	40.9	†	7.3 ± 0.6			
A-$^{13}C_2$	22	3	19	–	21	3	18	–	263 026.207	342.3	56.1	263 025.8	7.5 ± 0.6	0.14	0.10	
E-$^{13}C_2$	22	3	19		21	3	18		263 484.906	441.3	56.1	263 484.6	7.4 ± 0.6	0.10	0.11	

Table 5. continued.

Spec.	J	K_a	K_c	p	J'	K'_a	K'_c	p'	Calc. freq. (MHz)	E_u (K)	$S_{ij}\mu^2$ (D^2)	Obs. freq. (MHz)	v_{LSR} (km s^{-1})	T_{mb}^{obs} (K)	T_{mb}^{mod} (K)	Blend
E-^{13}C$_1$	23	–3	21		22	–3	20		264 936.868	350.6	60.7	264 936.9	7.0 ± 0.6	0.13	0.12	
E-^{13}C$_1$	7	–7	1		6	–6	1		264 937.868	236.2	3.22	†	8.1 ± 0.6			
A-^{13}C$_1$	24	2	23	–	23	2	22	–	265 443.450	354.0	63.8	265 442.1	8.5 ± 0.6	0.11	0.11	DCOOCH$_3$
A-^{13}C$_2$	22	6	17	–	21	6	16	–	265 640.606	356.9	53.7	265 640.8	6.8 ± 0.6	0.14	0.08	CH$_3$COOCH$_3$
E-^{13}C$_1$	25	–1	25		24	0	24		266 482.702	356.6	11.5	266 483.3	6.3 ± 0.6	0.35	0.29	
E-^{13}C$_1$	25	0	25		24	0	24		266 482.602	356.6	67.6	†	6.2 ± 0.6			
E-^{13}C$_1$	25	0	25		24	–1	24		266 482.416	356.6	11.5	†	6.0 ± 0.6			
E-^{13}C$_1$	25	–1	25		24	–1	24		266 482.517	356.6	67.6	†	6.1 ± 0.6			
A-^{13}C$_1$	22	10	13	–	21	10	12	–	267 355.733	400.6	47.3	267 355.8	6.9 ± 0.6	0.19	0.13	
A-^{13}C$_1$	22	10	12	+	21	10	11	+	267 355.808	400.6	47.3	†	7.0 ± 0.6			
E-^{13}C$_2$	23	–4	20		22	–4	19		270 150.708	454.7	58.5	270 152.0	5.6 ± 0.6	0.17	0.11	
A-^{13}C$_2$	23	3	20	–	22	3	19	–	272 723.937	355.4	58.5	272 723.7	7.3 ± 0.6	0.15	0.10	
A-^{13}C$_2$	26	0	26	+	25	0	25	+	272 941.805	367.2	68.3	272 941.8	7.0 ± 0.5	0.17	0.27	
A-^{13}C$_2$	26	1	26	+	25	0	25	+	272 941.891	367.2	11.7	†	7.1 ± 0.5			
A-^{13}C$_2$	26	0	26	+	25	1	25	+	272 941.649	367.2	11.7	†	6.9 ± 0.5			
A-^{13}C$_2$	26	1	26	+	25	1	25	+	272 941.735	367.2	68.3	†	7.0 ± 0.5			
A-^{13}C$_2$	23	16	8	–	22	16	7	–	274 076.953	515.3	31.4	274 077.0	7.0 ± 0.5	0.11	0.05	
A-^{13}C$_2$	23	16	7	+	22	16	6	+	274 076.953	515.3	31.4	†	7.0 ± 0.5			
A-^{13}C$_2$	23	15	8	–	22	15	7	–	274 124.220	494.7	35.1	274 125.7	5.4 ± 0.5	0.21	0.06	U
A-^{13}C$_2$	23	15	9	+	22	15	8	+	274 124.220	494.7	35.1	†	5.4 ± 0.5			
E-^{13}C$_1$	23	–4	20		22	–4	19		274 172.892	358.8	60.0	274 173.3	6.6 ± 0.5	0.23	0.11	
A-^{13}C$_2$	23	11	12	–	22	11	11	–	274 666.966	425.6	47.0	274 666.7	7.3 ± 0.5	0.24	0.12	
A-^{13}C$_2$	23	11	13	+	22	11	12	+	274 666.961	425.6	47.0	†	7.3 ± 0.5			
A-^{13}C$_2$	23	10	14	–	22	10	13	–	274 998.925	411.7	49.4	274 998.3	7.7 ± 0.5	0.35	0.13	CH$_3$OCH$_3$
A-^{13}C$_2$	23	10	13	+	22	10	12	+	274 999.054	411.7	49.4	†	7.9 ± 0.5			
E-^{13}C$_1$	23	3	20		22	3	19		276 849.213	358.5	60.1	276 849.6	6.5 ± 0.5	0.24	0.11	
E-^{13}C$_1$	26	–1	26		25	–1	25		276 936.143	369.9	70.3	276 934.7	8.5 ± 0.5	0.31	0.29	CH$_3$CH$_2$OH
E-^{13}C$_1$	26	0	26		25	0	25		276 936.189	369.9	70.3	†	8.6 ± 0.5			
E-^{13}C$_1$	26	0	26		25	–1	25		276 936.089	369.9	12.0	†	8.5 ± 0.5			
E-^{13}C$_1$	26	–1	26		25	0	25		276 936.244	369.9	12.0	†	8.7 ± 0.5			
E-^{13}C$_2$	24	–4	21		23	–4	20		280 723.536	468.2	61.1	280 722.7	7.9 ± 0.5	0.22	0.11	

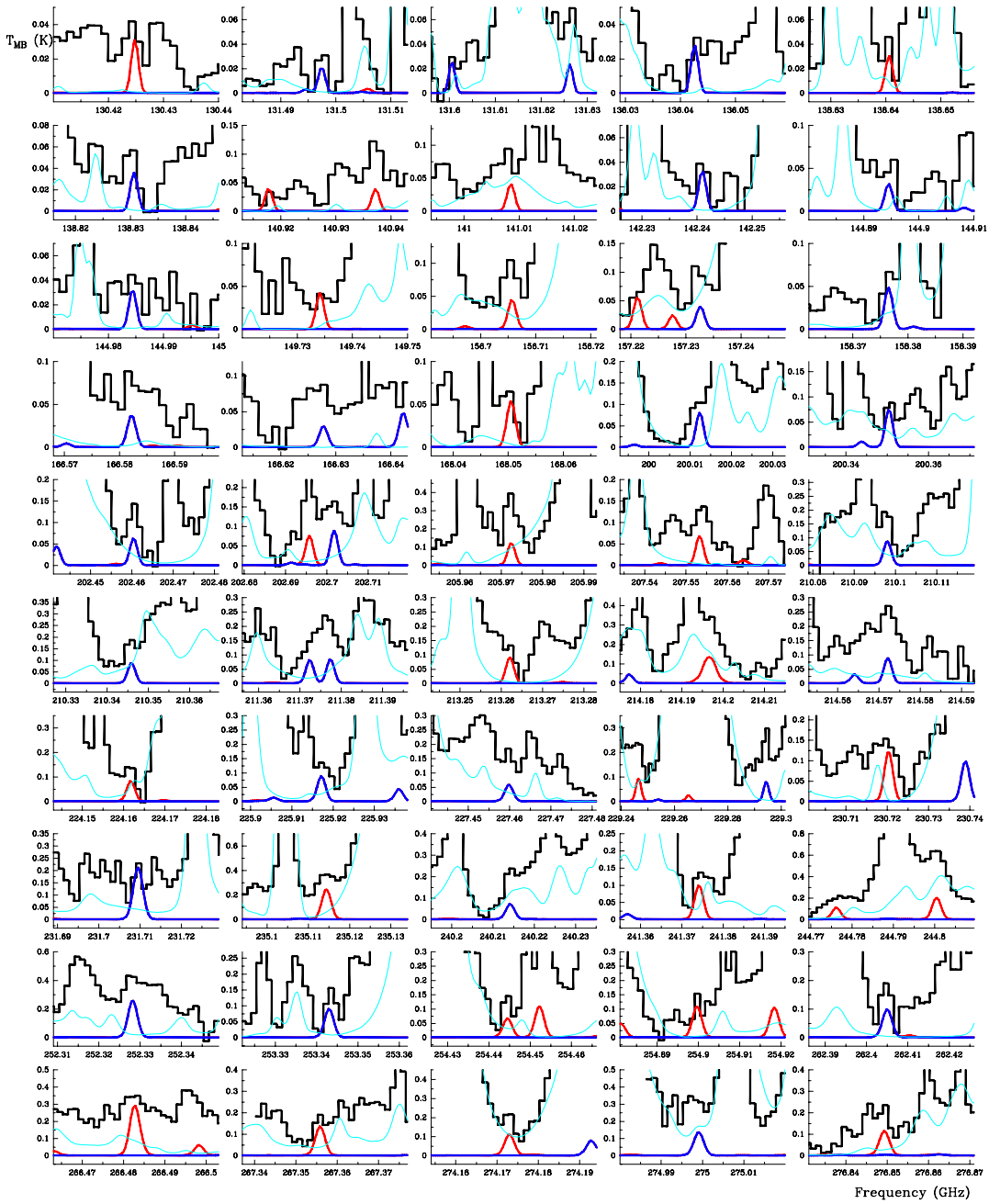

Fig. 2. Selected lines of A/E-$H^{13}COOCH_3$ $v_t = 1$ (modelled in red) and A/E-$HCOO^{13}CH_3$ $v_t = 1$ (modelled in dark blue) toward Orion-IRc2. The continuous cyan line corresponds to all lines already modelled in our previous papers except $H^{13}COOCH_3$ and $HCOO^{13}CH_3$ $\nu_t = 1$ (see Sect. 5.1). A v_{LSR} of 7 km s^{-1} is assumed.

has to be considered as the total intensity of the detected feature and an upper limit for the intensity of the methyl formate species in this study. Nevertheless, in Table 5 we found some values of the T_{mb}^{obs} lower than those predicted by the model (synthetic spectrum $HCOO^{13}CH_3$ and $H^{13}COOCH_3$ $\nu_t = 1$); uncertainties in the removed baselines are the most probable source for these discrepancies. The uncertainty in the radial velocity was adopted from the spectral resolution of our data. Most unblended detected lines show a radial velocity of $\simeq$7 km s^{-1}, in agreement with the expected velocity for emission from the compact ridge component where organic saturated O-rich molecules have the largest abundances inside the region. In addition, most detected lines of methyl formate, its isotopologues, and its first vibrationally excited state appear at the same radial velocity (see e.g. Carvajal et al. 2009; Margulès et al. 2010; Favre et al. 2011; Tercero et al. 2012; López et al., in prep.).

5.3. Modelling the data

To model the emission of $H^{13}COOCH_3$ and $HCOO^{13}CH_3$ $\nu_t = 1$ we used an excitation and radiative transfer code: MADEX (Cernicharo 2012). This time we applied LTE conditions because we lacked collisional rates for these species. Two compact ridge components (v_{LSR} = 7 km s^{-1} and $\Delta v = 3$ km s^{-1}) are enough to model the line profiles: one at 110 K, with diameter of 15″, and a column density of $(6 \pm 3) \times 10^{13}$ cm^{-2} for each state (A and E) of each isotopologue, and a hotter and inner compact ridge at 250 K with a diameter of 10″, and a column

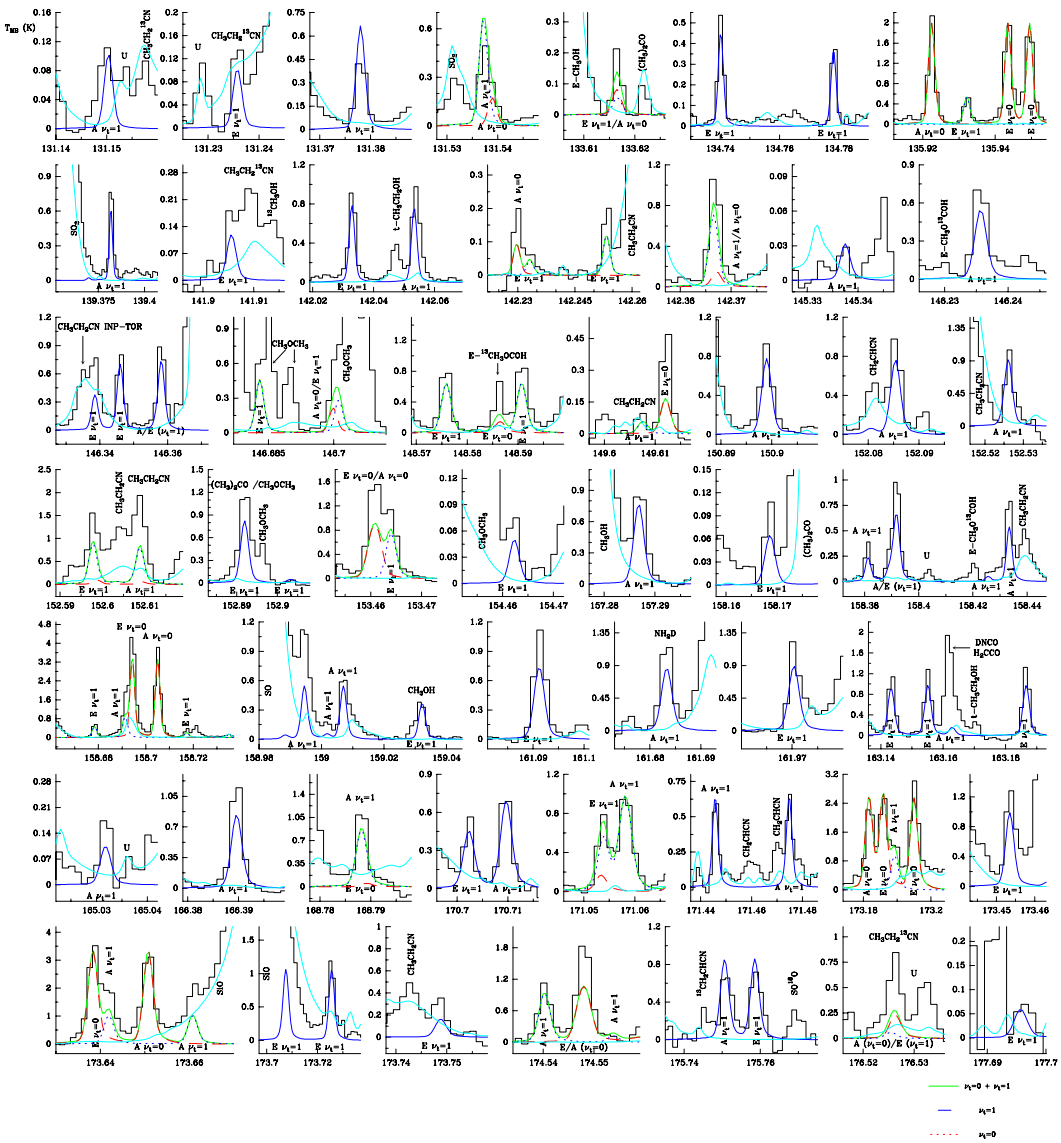

Fig. 3. Selected lines of A/E-HCOOCH$_3$ ν_t = 1 (modelled in dark blue) toward Orion-IRc2. The dashed red line and the green continuous line correspond to methyl formate in the ground state and the sum of the emission of v_t = 1 and v_t = 0, respectively. The continuous cyan line corresponds to all lines already modelled in our previous papers except HCOOCH$_3$ ν_t = 0, 1 (see Sect. 5.1). A $v_{\rm LSR}$ of 9 km s^{-1} is assumed. The x-axis is the frequency in GHz.

density of $(6 \pm 3) \times 10^{14}$ cm^{-2} for each state (A and E) of each isotopologue (both components are 7″ offset from the pointing position; interferometric maps show this component offset ≃7″ southwest from the source I – located 0.5″ south of IRc2, Menten & Reid 1995; see e.g. Neill et al. 2013 for ALMA cycle 0 maps). The beam dilution for each line (depending on the frequency) has been also taken into account in the calculation of the emerging line intensities. The obtained synthetic spectra is shown in Fig. 2. We obtained source averaged-column densities over the source size given for each component. Uncertainties of the column density results were estimated to be between 20−30% for this line survey (see Tercero et al. 2010) taking into account errors introduced by different sources, such as the spatial overlap of the different cloud components, the modest angular resolution, or pointing errors. Nevertheless, high overlap problems add another source of uncertainty (rising to 50%) for results obtained by means of weak lines such as those of H^{13}COOCH$_3$ and HCOO^{13}CH$_3$ v_t = 1. All together we obtained a total column density of $(1.4 \pm 0.7) \times 10^{15}$ cm^{-2} for each ^{13}C isotopologue of vibrationally excited methyl formate.

5.3.1. Isotope ratios

To obtain the ^{12}C/^{13}C ratio, we included our model for A/E-HCOOCH$_3$ v_t = 1 (López et al., in prep.). Figure 3 shows selected lines of methyl formate in its first vibrationally excited state in the 2 mm window (from 130 to 178 GHz). We modelled these species assuming all components listed in Table 4 and the hotter and inner compact ridge described above. The differences between the considered components with respect to the model of the ^{13}C isotopologues arise because the much more stronger lines of the main isotopologue in all the spectral band (from 80 to 280 GHz) allow us to distinguish the contribution of several cloud components in the line profiles, although some of them, such as the plateau contribution, are very low. For

$HCOOCH_3$ $v_t = 1$ we obtained a total column density of $(1.9 \pm 0.6) \times 10^{16}\,cm^{-2}$.

The column density ratio between the two vibrationally excited isotopologues (main and ^{13}C) of methyl formate yields a $^{12}C/^{13}C$ ratio between 6−35 (considering the error bars and assuming the same partition function for both species). Taking into account the weakness of the ^{13}C lines, the derived ratios are compatible with the value of $^{12}C/^{13}C \simeq 35$ obtained with the column density ratios between ^{13}C-$HCOOCH_3$ and $HCOOCH_3$ in the ground state (see Carvajal et al. 2009; Margulès et al. 2010) and agrees quite well with previous results of this ratio in Orion KL (Johansson et al. 1984; Blake et al. 1987; Demyk et al. 2007; Tercero et al. 2010; Daly et al. 2013; Esplugues et al. 2013b).

5.3.2. Vibrational temperatures

We can estimate vibrational temperatures from

$$\frac{\exp\left(-\frac{E_{v_t=1}}{T_{\rm vib}}\right)}{f_\nu} = \frac{N(^{13}C - HCOOCH_3\ \ v_t = 1)}{N(^{13}C - HCOOCH_3)}, \quad (1)$$

where $E_{v_t=1}$ is the energy of the vibrational state (187.6 K), $T_{\rm vib}$ is the vibrational temperature, f_ν is the vibrational partition function, $N(^{13}C\text{-}HCOOCH_3\ v_t = 1)$ is the column density of the vibrational state, and $N(^{13}C\text{-}HCOOCH_3)$ is the total column density of ^{13}C methyl formate. Taking into account that $N(^{13}C\text{-}HCOOCH_3) = N(\text{ground}) \times f_\nu$ and assuming the same partition function for these species in the ground- and the first vibrationally excited states, we only need the energy of the vibrational state and the column densities of ^{13}C-$HCOOCH_3$ $v_t = 1$ and ^{13}C-$HCOOCH_3$ $v_t = 0$ to derive the vibrational temperatures.

In Carvajal et al. (2009) we did not consider the hotter component of the compact ridge for column density calculations. After several works on methyl formate (Carvajal et al. 2009; Margulès et al. 2010; Tercero et al. 2012; Coudert et al. 2013; López et al., in prep.) we realize that this hotter component plays an important role in the global analysis of this molecule. In Margulès et al. (2010) we introduced a hot compact ridge to model the lines of main isotopologue of the methyl formate to properly reproduce the line profiles. After that, the study of the vibrationally excited states (this work and A. López et al., in prep.) confirms that a hot compact ridge is needed to understand the emission of this molecule. Therefore, quite strong lines such as those of ^{13}C-$HCOOCH_3$ require the hot compact ridge component to obtain the best fit. Consequently, here we again modeled the emission from $H^{13}COOCH_3$ and $HCOO^{13}CH_3$ taking into account a compact ridge at a temperature of 250 K and a source size of 10″. As in Carvajal et al. (2009), all cloud components of Table 4 where taken into account to reproduce the line profiles. Using MADEX and assuming LTE conditions, the obtained column densities for each ^{13}C isotopologue and each state (A and E) are $(2.0 \pm 0.6) \times 10^{15}\,cm^{-2}$ and $(2.0 \pm 0.6) \times 10^{14}\,cm^{-2}$ for the $T = 250$ K compact ridge and the $T = 110$ K compact ridge, respectively, and $(1.0 \pm 0.3) \times 10^{13}\,cm^{-2}$ for the plateau, the extended ridge, and the hot core. These values yield a total column density of a factor 3 higher than obtained in Carvajal et al. (2009). This difference is mostly due to the reduced source size when we introduced the hotter component of the compact ridge.

At this point, we were ready to derive the vibrational temperatures. We assumed that both gases (ground-state and vibrationally excited) are spatially coincident, so the calculated vibrational temperatures have to be considered as lower limits. A $T_{\rm vib} = 156$ K was obtained for $H^{13}COOCH_3$ and $HCOO^{13}CH_3$ $v_t = 1$ in each compact ridge component. This value is similar to the averaged kinetic temperature we adopted in this model (180 K). This result indicates that collisions are probably the main mechanism to populate the vibrationally excited levels of methyl formate.

6. Conclusion

We measured the spectra of $HCOO^{13}CH_3$ from 75 to 940 GHz. We analyzed 2881 lines from the first excited torsional states, 5728 new lines corresponding to the ground-vibrational states were also measured and added to the previous ones from Carvajal et al. (2009). The global fit of the 9455 lines, taking into account the internal rotation motion, was made using the rho-axis-method and the BELGI code. Fifty-two parameters could be determined, the global fit of both states permitted us to obtain uncorrelated values of the torsional parameters: F, V_3, and V_6. The value of barrier height ($V_3 = 369.93168(395)\ cm^{-1}$) has been significantly improved.

Owing to this work and Carvajal et al. (2009), accurate predictions of line positions and intensities were performed. In the line survey of Orion-KL with the IRAM 30 m telescope, this permits detecting 135 spectral features in the range 80−280 GHz; there are no missing transitions in this range. This is the first detection of an excited vibrational state of a methyl formate isotopologue.

At the beginning of the line identification process of this line survey (in 2005), nearly 8000 spectral features were U lines. In 2007 we began a close collaboration between astronomers and spectroscopists to reduce the uncertainty due to unidentified lines in spectral surveys. New isotopologues of ethyl cyanide and methyl formate (Demyk et al. 2007; Margulès et al. 2009, 2010; Carvajal et al. 2009; Tercero et al. 2012; Coudert et al. 2013) and new vibrationally excited states of formamide (Motiyenko et al. 2012), ethyl cyanide (Daly et al. 2013), and vinyl cyanide (López et al. 2014) have been studied in spectroscopy laboratories and detected in Orion KL for the first time space. Altogether, we reduced 3000 of unidentified lines through these studies. At this point, we were ready to search for new molecular species, detecting methyl acetate and *gauche*-ethyl formate (Tercero et al. 2013) and *gauche*-ethyl mercaptan (Kolesniková et al. 2014) for the first time in space, and providing the tentative detection of phenol (Kolesniková et al. 2013). These new species together with the work of López et al. (in prep., about vibrationally excited CH_3OCOH and CH_3COOH) account for ≃1000 lines. Up to date, we have reduced 4000 of U lines in the survey of Orion KL. We expect that a large number of the still unidentified lines arise from vibrationally modes of abundant species. However, low-lying vibrationally excited states of abundant molecules such as ethyl cyanide (for example the $\nu_{13} = 2/\nu_{21} = 2$ state at ~420 cm^{-1}) or methanol are still only poorly characterized in the laboratory, and certainly contribute to the remaining U-lines. The main goal of our studies is to provide the community with a fully analysed line survey of Orion that will constitute a template for ALMA observations of warm clouds.

Acknowledgements. M.C. acknowledges the financial support the Spanish Government through grant FIS2011-28738-C02-02, and by a joint project within the framework of a CNRS (France) and CSIC (Spain) agreement (Code No.: 2011 FR0018). J.C., A.L. and B.T. thank the Spanish MINECO for funding support from grants CSD2009-00038, AYA2009-07304, and AYA2012-32032. This work was supported by the Centre National d'Etudes Spatiales (CNES) and the Action sur Projets de l'INSU, "Physique et Chimie du Milieu Interstellaire". This work was also performed under the ANR-08-BLAN-0054.

Appendix A: Part of the supplementary tables available at the CDS

Table A.1. Assignments, observed frequencies, and calculated frequencies from the RAM fit, residuals, line strengths, and lower energy levels for methyl formate ($HCOO^{13}CH_3$) microwave transitions from $v_t = 0$ and $v_t = 1$ torsional states included in the fit with parameters of Table 2.

Upper state[a]					Lower state[a]										
v_t'	J'	K_a'	K_c'	p'	v_t''	J''	K_a''	K_c''	p''	Obs. Freq. (Unc.)[b]	Calc. Freq (Unc.)[c]	Obs.-Calc[d]	$S(i \rightarrow f)$[e]	Lower energy[f]	Ref[g]
1	50	0	50	+	1	49	0	49	+	519 745.410(30)	519 745.377(5)	0.033	137.102	560.0328	NEW B
1	51	0	51	+	1	50	0	50	+	530 000.398(30)	530 000.382(5)	0.016	22.972	577.3696	NEW B
1	52	0	52	+	1	51	0	51	+	540 252.626(30)	540 252.652(5)	–0.026	153.599	595.0485	NEW B
1	53	0	53	+	1	52	0	52	+	550 502.111(30)	550 502.133(6)	–0.022	154.358	613.0694	NEW B
1	54	0	54	+	1	53	0	53	+	560 748.773(30)	560 748.773(6)	0.000	137.761	631.4322	NEW B
1	55	0	55	+	1	54	0	54	+	570 992.521(30)	570 992.518(7)	0.003	148.615	650.1368	NEW B
1	56	0	56	+	1	55	0	55	+	581 233.298(30)	581 233.318(7)	–0.020	35.289	669.1830	NEW B
1	57	0	57	+	1	56	0	56	+	591 471.082(30)	591 471.118(8)	–0.036	181.673	688.5709	NEW B
1	58	0	58	+	1	57	0	57	+	601 705.819(30)	601 705.866(9)	–0.047	184.679	708.3002	NEW B
1	59	0	59	+	1	58	0	58	+	611 937.436(30)	611 937.510(10)	–0.074	187.823	728.3710	NEW B
1	60	0	60	+	1	59	0	59	+	622 165.944(30)	622 165.996(11)	–0.052	190.689	748.7830	NEW B
1	50	0	50		1	49	0	49		519 732.280(30)	519 732.271(5)	0.009	159.484	559.5257	NEW B
1	51	0	51		1	50	0	50		529 985.311(30)	529 985.287(6)	0.024	161.679	576.8621	NEW B
1	52	0	52		1	51	0	51		540 235.593(30)	540 235.566(6)	0.027	122.669	594.5405	NEW B
1	53	0	53		1	52	0	52		550 483.081(30)	550 483.060(6)	0.021	114.755	612.5608	NEW B
1	54	0	54		1	53	0	53		560 727.716(30)	560 727.709(6)	0.007	172.372	630.9230	NEW B
1	55	0	55		1	54	0	54		570 969.450(30)	570 969.463(7)	–0.013	175.587	649.6268	NEW B
1	56	0	56		1	55	0	55		581 208.238(30)	581 208.268(7)	–0.030	178.795	668.6723	NEW B
1	57	0	57		1	56	0	56		591 444.057(30)	591 444.072(8)	–0.015	182.011	688.0593	NEW B
1	58	0	58		1	57	0	57		601 676.811(30)	601 676.819(9)	–0.008	185.223	707.7878	NEW B
1	59	0	59		1	58	0	58		611 906.456(30)	611 906.456(9)	0.000	188.431	727.8576	NEW B
1	60	0	60		1	59	0	59		622 132.891(30)	622 132.935(10)	–0.044	191.656	748.2686	NEW B

Notes. [a] Upper and lower state quantum numbers are indicated by $'$ and $''$ respectively. Torsion-rotation levels of A species have a "parity" label; levels of E species have a signed K_a value (Herbst et al. 1984). [b] Observed $v_t = 0$ and 1 microwave transitions in MHz, with estimated uncertainties in parentheses (in kHz). [c] Calculated line frequency in MHz with calculated uncertainty in kHz. [d] Differences among the experimental and computed frequencies. [e] Calculated line strengths in D**2 (for details of the calculation procedure, see Sect. 4). [f] Lower state energy (cm^{-1}) referred to the $J = K_a = 0$ A-species energy level taken as the zero of the energy (zero-point torsional energy: 71.0704 cm^{-1}). [g] Sources of data are explained in footnote b of Table 1. Blended lines are indicated with a capital letter B.

References

Bell, T. A., Cernicharo, J., Viti, S., et al. 2014, A&A, 564, A114
Blake, G. A., Sutton, E. C., Masson, C. R., & Philips, T. H. 1987, ApJ, 315, 621
Brown, R. D., Crofts, J. G., Gardner, F. F., et al. 1975, ApJ, 197, L29
Churchwell, E., & Winnewisser, G. 1975, A&A, 45, 229
Carvajal, M., Willaert, F., Demaison, J., & Kleiner, I. 2007, J. Mol. Spectrosc., 246, 158
Carvajal, M., Margulès, L., Tercero, B., et al. 2009, A&A, 500, 1109
Carvajal, M., Kleiner, I., & Demaison, J. 2010, ApJS, 190, 315
Cernicharo 1985, Internal IRAM report (Granada: IRAM)
Cernicharo, J. 2012, in ECLA-2011: Proc. of the European Conf. Laboratory Astrophysics, EAS Publ. Ser., eds C. Stehl, C. Joblin, & L. d'Hendecourt (Cambridge: Cambridge Univ. Press), 251
Cernicharo, J., Tercero, B., Fuente, A., et al. 2013, ApJ, 771, L10
Comito, C., Schilke, P., Phillips, T. G., et al. 2005, ApJS, 156, 127
Coudert, L. H., Drouin, B. J., Tercero, B., et al. 2013, ApJ, submitted
Curl, R. F. 1959, J. Chem. Phys., 30, 1529
Daly, A. M., Bermúdez, C., López, A., et al. 2013, ApJ, 768, 81
Demyk, K., Mäder, H., Tercero, B., et al. 2007, A&A, 466, 255
Demyk, K., Wlodarczak, G., & Carvajal, M. 2008, A&A, 489, 589
Esplugues, G. B., Tercero, B., Cernicharo, J. et al. 2013, A&A, 556, A143
Esplugues, G. B., Cernicharo, J., Viti, S., et al. 2013, A&A, 559, A51
Favre, C., Despois, D., Brouillet, N., et al. 2011, A&A, 532, A32
Favre, C., Carvajal, M., Field, D., et al. 2014, ApJ, submitted
Groner, P. 1997, J. Chem. Phys., 107, 4483
Groner, P. 2012, J. Mol. Spectrosc., 278, 52
Haykal, I., Motiyenko, R. A., Margulès, L., & Huet, T. R. 2013a, A&A, 549, A96
Haykal, I., Margulès, L., Motiyenko, R. A., et al. 2013b, ApJ, 777, 120
Herbst, E., Messer, J. K., De Lucia, F. C., & Helminger, P. 1984, J. Mol. Spectrosc., 108, 42
Hougen, J. T., Kleiner, I., & Godefroid, M. 1994, J. Mol. Spectrosc., 163, 559
Ilyushin, V., Alekseev, E. A., Dyubko, S. F., & Kleiner, I. 2003, J. Mol. Spectrosc., 220, 170
Ilyushin, V., Kleiner, I., & Lovas, F. J. 2008, J. Phys. Chem. Ref. Data, 37, 97
Ilyushin, V. V., Kryvda, A., & Alekseev, E. 2009, J. Mol. Spectrosc., 255, 32
Johansson, L. E. B., Andersson, C., Elldér, J., et al. 1984, A&A, 130, 227
Kirtman, B. 1962, J. Chem. Phys., 37, 2516
Kleiner, I. 2010, J. Mol. Spectrosc., 260, 1
Kleiner, I., Hougen, J. T., Grabow, J. U., et al. 1996, J. Mol. Spectrosc., 179, 41
Kobayashi, K., Ogata, K., Tsunekawa, S., & Takano, S. 2007, ApJ, 657, L17
Kolesniková, L., Daly, A. M., Alonso, J. L., Tercero, B., & Cernicharo, J. 2013, J. Mol. Spectrosc., 289, 13
Kolesniková, L., Tercero, B., & Cernicharo, J. 2014, ApJ, 784, L7
Lees, R. M., & Baker, J. G. 1968, J. Chem. Phys., 48, 5299
Lin, C. C., & Swalen, J. D. 1959, Rev. Mod. Phys., 31, 841
López, A., Tercero, B., Kisiel, Z., et al. 2014, A&A, submitted
Maeda, A., Medvedev, I. R., De Lucia, F. C., & Herbst, E. 2008a, ApJS, 175, 138
Maeda, A., De Lucia, F. C., & Herbst, E. 2008b, J. Mol. Spectrosc., 251, 293
Margulès, L., Motiyenko, R. A., Demyk, K., et al. 2009, A&A, 493, 565
Margulès, L., Huet, T. R., Demaison, J., et al. 2010, ApJ, 714, 1120
Menten, K. M., & Reid, M. J. 1995, ApJ, 445, L157
Motiyenko, R. A., Margulès, L. , Alekseev, E. A., Guillemin, J.-C., & Demaison, J. 2010, J. Mol. Spectrosc., 264, 94.
Motiyenko, R. A., Tercero, B., Cernicharo, J., & Margulès, L. 2012, A&A, 548, A71
Neill, J. L., Crockett, N. R., Bergin, E. A., Pearson, J. C., & Xu, L.-H. 2013, ApJ, 777, 85
Oesterling, L. C., Ferguson, D. W., Herbst, E., & De Lucia, F. C. 1995, J. Mol. Spectrosc., 172, 469
Pardo, J. R., Cernicharo, J., & Serabyn, E. 2001, IEEE Tras. Antennas and Propagation, 49, 12
Persson, C. M., Olofsson, A. O. H., Koning, N., et al. 2007, A&A, 476, 807
Schilke, P., Benford, C. J., Hunter, T. R., Lis, D. C., & Philips, T. G. 2001, ApJS, 132, 281
Tercero, B. 2012, Ph.D., Univ. Complutense de Madrid
Tercero, B., Pardo, J. R., Cernicharo, J. R., & Goicoechea, J. R. 2010, A&A, 517, A96
Tercero, B., Vincent, L., Cernicharo, J., Viti, S., & Marcelino, N. 2011, A&A, 528, A26
Tercero, B., Margulès, L., Carvajal, M., et al. 2012, A&A, 538, A119
Tercero, B., Kleiner, I., Cernicharo, J., et al. 2013, ApJ, 770, L13
Tudorie, M., Ilyushin, V., Vander Auwera, J., et al. 2012, J. Chem. Phys., 137, 064304
Willaert, F., Møllendal, H., Alekseev, E., et al. 2006, J. Mol. Struct., 795, 4
Takano, S., Sakai, Y., Kakimoto, S., Sasaki, M., & Kobayasho, K. 2012, PASJ, 64, 89